THE HONG KONG
POLYTECHNIC UNIVERSITY
香港理工大學
Pao Yue-kong Library
包玉剛圖書館

Copyright Undertaking

This thesis is protected by copyright, with all rights reserved.

By reading and using the thesis, the reader understands and agrees to the following terms:

1. The reader will abide by the rules and legal ordinances governing copyright regarding the use of the thesis.
2. The reader will use the thesis for the purpose of research or private study only and not for distribution or further reproduction or any other purpose.
3. The reader agrees to indemnify and hold the University harmless from and against any loss, damage, cost, liability or expenses arising from copyright infringement or unauthorized usage.

If you have reasons to believe that any materials in this thesis are deemed not suitable to be distributed in this form, or a copyright owner having difficulty with the material being included in our database, please contact lbsys@polyu.edu.hk providing details. The Library will look into your claim and consider taking remedial action upon receipt of the written requests.

Pao Yue-kong Library, The Hong Kong Polytechnic University, Hung Hom, Kowloon, Hong Kong

http://www.lib.polyu.edu.hk

The Hong Kong Polytechnic University

Department of Civil and Structural Engineering

IDENTIFICATION OF THE EFFECT OF BIOMASS BURNING ON TRACE GASES AND AEROSOL AT THE REMOTE SITES OF CHINA

Wong Kam-hang Daniel

A thesis

submitted in partial fulfillment of the requirements for the Degree of

Master of Philosophy

January 2007

Pao Yue-kong Library
PolyU • Hong Kong

DECLARATION

I hereby declare that this thesis entitled "Identification of the effect of biomass burning on trace gases and aerosol at the remote sites of China" is my own work that, to the best of my knowledge and belief, it reproduces no material previously published or written, nor material that has been accepted for the award of any other degree or diploma, except where due acknowledgement has been made in the text.

_____

Wong Kam-hang Daniel

Abstract of thesis entitled "Identification of the effect of biomass burning on trace gases and aerosol at the remote sites of China" Submitted by Mr. Wong Kam-hang Daniel for the degree of Master of Philosophy at the Hong Kong Polytechnic University in January 2007.

The March-May months correspond to the transition from winter to summer monsoon season over Asia. As it progresses from winter to spring, convection becomes significant. Hence, pollution from Asia are mixed with the pollution from the west of China arrived with the westerly wind. At the same time, spring is the dry season in Southeast (SE) Asia. This season is favorable for the occurrence of forest fire. In addition, in late winter and early spring, people in the Asian subcontinent start to burn the crop residues of the previous year in preparation for cultivating of new crops. These fires very often become out of control. As a result, larger scale forest fires frequently occurred in Asia.

My study comprised two phases. During the first phase study in spring of 2004, surface ozone (O_3), carbon monoxide (CO) and aerosols over the Tibetan Plateau were measured at a remote site in the southwestern border of China. While at the second phase, surface O_3 and CO over the boreal forest region were measured in the same period in the spring of 2005 at a rural site in northeastern China.

In the spring of 2004, surface O_3, CO, and aerosols ($PM_{2.5}$ and PM_{10}) were measured within the southeastern Tibetan Plateau at Tengchong (25.01°N, 98.3°E, 1960 m a.s.l.) in Southwest China, where observational data is scarce. The O_3 level measured is low when compared with those reported in similar longitudinal sites in

SE Asia as well as in northeastern Tibetan Plateau in Northwest China suggesting that there exist complex O_3 variations in the Tibetan Plateau and its neighboring SE Asian region. The increase of pollutants in the lower troposphere was caused by regional built-up and transport of pollution from active biomass burning region.

In the spring of 2005, ground-based measurements of O_3 and CO were performed in Longfeng San World Meteorological Organization (WMO) Regional Background Station, which is located in Heilongjiang Province in northeastern China. At that time, Korean forest fires occurred. These forest fires destroyed more than 400 hectares of woodlands. Twenty one mountainous areas in Korea were engulfed. These forest fires released considerable amount of ozone precursors and particulates into the atmosphere and induced adverse effects on the regional air quality. With the help of satellite data, we found that under the influence of the low pressure system in northern China, the emissions from these forest fires traversed the Korean peninsula, and affected northeastern China.

This study provided measurement data at two remote sites of China, at the Tibetan Plateau in southwestern China and at the boreal forest in northeastern China, where observational data are scarce. In this regard, the measurements from this study may serve as a baseline against which future measurements and changes are compared and evaluated. Also, the impacts of open burning activities from neighboring Asian countries to China were assessed and analyzed in this study.

PUBLICATIONS ARISING FROM THE DISSERATION

A. Published proceedings in international conferences

1. **Wong, K.H**., C.Y. Chan, L.Y. Chan, Y.S. Li, "*Identification of the effect of biomass burning on trace gases and aerosol at a remote site of Southwest China"*, Workshop on Meteorology and Climate over South China, pp.16- 21, 5-8 Dec, 2005.
2. **Wong, K.H.** and L.Y. Chan, "*Transport of Air Pollution and Tropospheric Ozone over China (TAPTO-China) during the Spring of 2004*", The 4th WSEAS International Conference on Environment, Ecosystems and Development (EED'06), WSEAS TRANSACTIONS on Environment and Development, Issue 9, Vol. 2, pp.1209-1214, Sept 2006, ISSN 1790-5079.

B. Published research articles in international journals

1. Chan C.Y., **K.H. Wong**, L.Y. Chan, X.D. Zheng, Y.S. Li, "*The effects of Southeast Asia fire activities on tropospheric ozone, trace gases and aerosols at a remote site over the Tibetan Plateau of Southwest China"*, Tellus, 58B, 310-318, 2006.
2. **Wong, K.H.**, L.Y. Chan, Y.S. Li, C.Y. Chan, X.D. Zheng and C.S. Zhao, "*Effects of Korean Forest Fires on the atmosphere of Northeast China*", Tellus B, (submitted) .

ACKNOWLEDGMENTS

Words cannot be expressed in how I am indebted to Dr. L.Y. Chan, my chief supervisor, for his guidance and support in this project.

I would like to thank Prof. Y.S. Li, my co-supervisor, for all the wonderful opportunities and freedom he granted me throughout my graduate career in The Hong Kong Polytechnic University.

I greatly acknowledge Dr. S.C. Lee and Dr. K.F. Ho for carrying out the chemical analysis for my field samples. I also like to thank Mr. W.F. Tam for his technical assistance and support. Thanks also go to Dr. C.Y. Chan for his kindness in giving valuable comments.

I would also like to thank the personnel at the Tengchong Meteorological Station and, the Long Fengshan World Meteorological Organization (WMO) Regional Background Station for their help in the field experiment.

At last but not the least, I would like to say thank you to my family and my girlfriend, Miss W.M. Kwong, for their love and support.

This project is supported by the Research Grants Council of Hong Kong and a research grant of The Hong Kong Polytechnic University.

Table of Contents **Page**

CHAPTER

List of Tables

List of Figures

List of Appendices

CHAPTER 1 - OVERVIEW

1.1. Background of Research

Emissions from open burning, such as biomass burning and forest fire, are greater than those from well-controlled combustion sources. Biomass burnings and accidental forest fires can produce large amount of trace gases and mixtures of aerosol particles, such as soot, soluble organic compounds, sulfates, and nitrates. The gases and aerosols produced by the fires play important roles in the atmospheric chemistry, cloud microphysics and radiation balance in the lower atmosphere. So far, field measurements of key air pollutants in China have been comparatively sparse, especially in rural locations. In this study, trace gases and aerosol in selected sites of China were measured. The data collected will enable us to understand pollution problems in China and provide valuable data to elucidate atmospheric processes, to reconcile emission inventories, and to validate regional chemical transport models.

The Transport of Air Pollution and Tropospheric Ozone over China (TAPTO-China) is a field campaign to measure transboundary transport of air pollution from/across Southeast Asia, the Eurasia continent and China, and its impact on tropospheric O_3 and pollution outflow to the Pacific. The field campaign comprises two phases of experiment. In the first phase study in the spring of 2004, field measurements were performed along the major subtropical air mass transport pathway while in the spring of 2005, measurements were setup along the major mid-latitude air mass transport pathway trespassing China.

The Tibetan Plateau is the largest plateau in the world that exerts profound thermal and dynamic influences on local and global climate, and atmospheric circulation of the Asian Monsoon System. Each March and April, an air mass starts to inflow from the Indian Ocean through the Bay of Bengal and the Tibetan Plateau towards inland Asia. The water content, physical and chemical properties of the air mass have vital regional effect on the weather and climate of China and East Asia. However, field data of trace gases and aerosols that are chemically and radiatively important for the Tibetan Plateau are scare. My study performed in 2004 described and interpreted chemical measurements taken on the Tibetan Plateau of southwest China, a region that previously had been devoid of such measurements. This study provides information to fill the gap in one vacuum area of the Eurasian continent. The impacts of the biomass burning activities in South and Southeast Asia are also assessed.

In Northeastern China, less attention was paid to the impact of the emissions of forest fires from neighbor countries to the local atmosphere. In my study during the spring of 2005, intensive Korean forest fires during the Arbor Day in 2005 were observed. This study showed that, under influences of low pressure system in northern China, the emissions from these forest fires could traverse the Korean peninsula, and trespassed down to the northeastern part of China. To our best knowledge, it was the first record of adverse air pollution effect resulted from Korean forest fires over northeastern China.

1.2. Aims and Objectives

- To carry out field measurements of surface ozone and its precursors and aerosol in selected un-intruded and undeveloped regions of China.

- To explore the impact of open biomass burning activities on the air quality in selected sites of China during the springtime period.

- To assess the chemical and physical processes that control ozone formation and transport in these regions and thus to understand the contribution of ozone pollution in these regions.

1.3. Project Layout

In Chapter 2, a brief literature review on the global effects of emissions of open burnings to the atmosphere has been presented. It includes the historical review of the air pollution transport in South and North Asia. The descriptions of field measurements, additional data and the analysis methodology will be given in chapter 3. In Chapters 4 and 5, the field data collected in the springs of 2004 and 2005 are presented and analyzed. In Chapter 6, the major findings, the significant contributions and the implications of this study are highlighted.

CHAPTER 2 - LITERATURE REVIEW

2.1. Definition of biomass burning

Biomass burning is the combustion of organic matter. Burning can be from natural or man-made fires. It usually refers to the burning of the world's forests, grasslands and agricultural lands following harvest for the purpose of land clearing and land conversion. One form of the biomass burnings is forest fires which are a powerful emission source of atmospheric pollutants. Biomass burning is a major source of many atmospheric particulates and trace gases which influence the concentration of tropospheric ozone.

2.2. Emission from biomass burning

Biomass matter is mostly carbon. Estimates for the release of carbon (in units of teragrams of carbon, TgC/year, where 1 teragram equals 10^{12} grams or 10^{6} metric tons) into the atmosphere from biomass burning for different ecosystems are summarized in Table 2.1 (Andreae, 1991). Savanna fires and forest fires are two major types of biomass burning and were reported in many studies (Allen and Miguel, 1995; Andreae, 1991; Lacaux et al., 1993; Cachier et al., 1995). However, agricultural field burning is another type of biomass burning which may be regionally important during the harvest season. Most of the remainder of the biomass matter is water. Biomass matter also contains trace amounts of several other elements, including nitrogen, sulfur, chlorine, and bromine. During burning, these elements are volatilized and released into the atmosphere in the form of molecular nitrogen, nitric oxide, nitrous oxide, sulfur dioxide, methyl chloride, and methyl bromide. The contributions of biomass burning to the global emissions are summarized in Table 2.2 (Andreae, 1991).

Table 2.1. Global estimates of annual amounts of biomass burning and of the resulting release of carbon into the atmosphere (Andreae, 1991)

Source of burning	Biomass burned (Tg dry matter / year)	Carbon released (Tg carbon / year)
Savannas	3690	1660
Agricultural waste	2020	910
Tropical forests	1260	570
Fuel wood	1430	640
Temperate and boreal forests	280	130
Charcoal	30	21
World total	8700	3940

Table 2.2. Comparison of global emissions from biomass burning with emissions from all sources, including biomass burning (Andreae, 1991)

Species	Biomass burning (Tg element/year)	All sources (Tg element/year)	Biomass burning (%)
Carbon dioxide (gross)	3500	8700	40
Carbon dioxide (net)	1800	7000	26
Carbon monoxide	350	1100	32
Methane	38	380	10
Nonmethane hydrocarbons	24	100	24
Nitric oxide	8.5	40	21
Ammonia	5.3	44	12
Sulfur gases	2.8	150	2
Methyl chloride	0.51	2.3	22
Hydrogen	19	75	25
Tropospheric ozone	420	1100	38
Total particulate matter	104	1530	7
Particulate organic matter	69	180	39
Elemental carbon (black soot)	19	<22	>86

Emissions from open burning, on a mass pollutant per mass fuel (emission factor) basis, are greater than those from well-controlled combustion sources. Some types of open burning (e.g. biomass) are large sources on a global scale in comparison to other broad classes of sources (e.g. mobile and industrial sources). Lemieux et al. (2004) performed a detailed literature search reporting emissions of organic air toxic from open burning sources. Results indicated that biomass open burning sources typically emitted less Volatile Organic Compounds (VOCs) than open burning sources with anthropogenic fuels on a mass emitted per mass burned basis, particularly those where polymers were concerned. Biomass open burnings sources typically emitted less Semi-Volatile Organic Compounds (SVOCs) and Polycyclic Aromatic Hydrocarbons (PAHs) than anthropogenic sources on a mass emitted per mass burned basis. Burning pools of crude oil and diesel fuel produced

significant amounts of PAHs relative to other types of open burning. PAHs emissions were highest when combustion of polymers was taking place. Based on the available data, biomass open burning sources typically produced higher levels of carbonyls than anthropogenic sources on a mass emitted per mass burned basis, probably due to oxygenated structures resulting from thermal decomposition of cellulose.

Emissions from the burning of biomass are potentially major sources of air toxics. Table 2.3 summarized the emissions from prescribed burning and forest fires (mg/kg burned). Grasslands are burned for various reasons, including manipulating vegetation, enhancing biological productivity and biodiversity, prairie restoration and maintenance, reduction of woody plants, or management for endangered species (Higgins et al. 1989). Savanna and forest fires may also occur naturally through lightning strikes. These types of fires are dynamic events where a moving flame front passes over the fuel source, such as a savanna or forest. Because of this behavior, both smoldering and flaming combustion zones exist with each type of combustion dominating at different times. VOCs and SVOCs are emitted in large quantities with a large variety of oxygenated organic compounds from the thermal decomposition of cellulose.

Table 2.3. Emissions from prescribed burning and forest fires (mg/kg burned, Lemieux et al., 2004)

Class	Compound	Savanna and grassland	Tropical forest	Extratropical forest
VOCs	Batadiene	70		60
	Benzene	230	400	490
	Toluene	130	250	400
	Xylenes	45	60	200
	Ethylbenzene	13	24	48
	Styrene	24	30	130
	Methylchloride	75	100	50
	Methylbromide	2.1	7.8	3.2
	Methyliodide	0.5	6.8	0.6
	Acetonitrile	110	180	190
SVOCs	Furan	95	480	425
	2-Methylfuran	46	170	470
	3-Methylfuran	8.5	29	50
	2-Ethylfuran	1	3	6
	2,4-Dimethylfuran	8	24	19
	2,5-Dimethylfuran	2	30	50
	Tetrahydrofuran	16	16	20
	2,3-Dihydrofuran	12	13	17
	Benzofuran	14	15	26
	Furfural	230	370	460
	PAH	2.4	25	25
	Phenol	3	6	5
Carbonyls	Methanol	1300	2000	2000
	Formaldehyde	350	1400	2200
	Acetaldehyde	500	650	500
	Acrolein	80	180	240
	Propionaldehyde	9	80	140
	Butanals	53	71	210
	Hexanals	13	31	20
	Heptanals	3	3	4
	Acetone	435	620	555
	Methylehtylketone	260	430	455
	2,3-Butanedione	570	920	925
	Pentanones	15	28	90
	Heptanones	6	2	5
	Octanones	15	19	20
	Benzaldehyde	29	27	36

2.3. Global effects of emissions of open burnings to the atmosphere

Biomass burning has drawn global concerns in the past decades for its effects on visibility, human health and global climate by releasing the gases and particulates into the atmosphere (Andreae, 1991; Fang et al., 1999; Radojevic, 1997, Koe et al., 2001). The instantaneous combustion products of burning vegetation include carbon dioxide, carbon monoxide (CO), methane, nonmethane hydrocarbons, nitric oxide, methyl chloride, and various particulates. The gases produced by biomass burning are environmentally significant. The greenhouse gases, carbon dioxide and methane, influence global climate. Combustion particulates affect the global radiation budget and climate. Carbon monoxide, methane, nonmethane hydrocarbons, and nitric oxide are all chemically active gases that affect the oxidizing capacity of the atmosphere and lead to the photo-chemical production of ozone in the troposphere. The detailed formation mechanisms will be discussed in section 2.5. Methyl chloride is a source of chlorine to the atmosphere, which leads to the chemical destruction of stratospheric ozone. Recently, it was discovered that biomass burning is also an important global source of atmospheric bromine in the form of methyl bromine (Mann and Andreae, 1994). Bromine leads to the chemical destruction of ozone in the stratosphere and is about 40 times more efficient in that process than is chlorine on a molecule-for-molecule basis.

During the burning of a forest, carbon dioxide that was sequestered for periods ranging from decades to centuries is suddenly released and returned to the atmosphere in a matter of hours. The burning of forests also destroys an important sink for atmospheric carbon dioxide. Hence, burning has both short- and long-term

impacts on the global carbon dioxide budget. If the burned vegetation is not re-grown, the liberated carbon dioxide remains in the atmosphere. If the burned ecosystem re-grows, as the savannas do, the carbon dioxide is eventually removed from the atmosphere via photosynthesis and is incorporated into the new vegetative growth. Other gaseous emissions, however, remain in the atmosphere.

2.4. Identification of biomass burnings contributing to the enhancement of air pollution

2.4.1 Tracers of biomass burnings in gaseous samples

Biomass burning is an important source of global trace gases and aerosols. It had been estimated that biomass burning emitted about 38.0 Tg of Non-Methane Hydrocarbons (NMHCs) in 2000 (Ito and Penner, 2004). Therefore, the source apportionments from selected hydrocarbons are widely used to identify the emissions from anthropogenic sources. Choi et al. (2003) reported the qualitative source apportionment for selected hydrocarbons and they were summarized in Table 2.4. Fossil fuel combustion, biomass burning, natural gas and liquefied petroleum gas (LPG) are the major sources of ethane, while natural gas, LPG and biomass burning are the major sources of propane (Choi et al., 2003). The ethane/propane ratio can thus reflect the differences in contribution of biomass burning, biofuel combustion and transportation. High value indicates regions with tropical forests fire and large biomass burnings. Intermediate value reflects a blend of biofuel and biomass usage, and the small value reflects industrial regions dominated by fossil fuel usage (Carmichael et al. 2003). Carmichael et al. (2003) reported an ethane/propane ratio of 8 in the SE Asian biomass burning plumes, 2.3 in biofuel combustion exhaust and 0.5 in traffic affected air. They also reported a ratio of 1 to 6 during the TRACE-P campaign. Based on the anthropogenic emission inventory, Russo et al. (2003) estimated the ethane/propane ratio was 2.1 in China and 3.8 in SE Asia. Wang et al. (2003, 2005) reported a C_2H_6/C_3H_8 ratio of 2.6-2.7 in the air

mass from local urban region and mainland China, 3.1 from the coast of mainland China in Hok Tsui, 2.7 in Linan (a rural site in Eastern China) and 1.6 in Tai O (a rural site of Hong Kong).

Table 2.4. Qualitative source apportionment for selected hydrocarbons.

Hydrocarbon	Sources
Methane	Managed and natural wetlands, enteric fermentation, landfills, human and animal waste, natural gas, coal combustion
Ethane	Fossil fuel combustion, natural gas, liquefied petroleum gas, biomass burning, the ocean, grasses and other vegetation
Propane	Natural gas, liquefied petroleum gas, biomass burning, the ocean grasses and other vegetation
n-Butane	Fossil fuel combustion, natural gas, liquefied petroleum gas, biomass burning, the ocean
i-Butane	Fossil fuel combustion, natural gas, liquefied petroleum gas, biomass burning, the ocean
n-Pentane	Fossil fuel combustion, natural gas, liquefied petroleum gas
i-Pentane	Fossil fuel combustion, natural gas, liquefied petroleum gas
Ethene	Fossil fuel combustion, biomass burning, the ocean, vegetation
Propene	Fossil fuel combustion, biomass burning, the ocean
Ethyne	Fossil fuel combustion, biomass burning
Benzene	Fossil fuel combustion, biomass burning, solvents
Toluene and Xylenes	Fossil fuel combustion, solvents, biomass burning

2.4.2. Tracers of biomass burnings in aerosol samples

Organic carbon (OC) and water-soluble potassium (K^+) are the typical components of biomass burning aerosol. Close to fires, OC is accounted for about two-third of biomass burning aerosol mass (Cachier et al., 1995). K^+ has been used as tracer element for the qualitative identification of biomass burning (Cachier et al., 1991; Chow, 1995), in source apportionment study (Lewis et al., 1988), as well as for wood smoke in receptor models (Echalar et al., 1995). As biomass burning combustion sources are generally featured by high K^+ contents (Cachier et al., 1991; Andreae and Merlet, 2001), the K^+/OC ratio could be an indicator to help distinguish

biomass burning from other OC sources. In addition, K^+/OC ratio could be used to distinguish the types of biomass burning. Echalar et al. (1995) and Maenhaut et al. (1996) indicated that savanna burning emissions during their flaming phase produce K^+ and OC in the proportion of 0.08-0.10. Andreae and Merlet (2001) estimated the K^+/OC ratio for agricultural residues burning in the same range (0.04-0.13). Duan et al. (2004) reported that the higher K^+/OC ratio (0.19-0.21) could be representative for on-field wheat straw open fires.

The major natural sources for particulate K^+ are sea salts and soils, and biomass burning constitutes the major part of its anthropogenic source (Echalar et al., 1995). In order to separate the contribution of sea-salt and non-sea-salt K^+, the concentration of non-sea salt K^+ (nss-K^+) are calculated by equation [2.1] and by assuming that the chemical composition of sea-salt particles is the same as that of sea water, and that the soluble Na^+ in particulate samples comes solely from sea-salts (Kennish, 1994).

$$\text{nns-}K^+ = [K^+] - [Na^+]0.037 \qquad [2.1]$$

2.5. Formation of O_3 by biomass burning emissions in the lower atmosphere

In the lower atmosphere, the only significant process forming O_3 is the photolysis of NO_2, which is reversed by the rapid reaction of O_3 with NO (Carter, 1994).

$$NO_2 + hv \rightarrow O(^3P) + NO$$

$$O(^3P) + O_2 + M \rightarrow O_3 + M$$

$$O_3 + NO \rightarrow NO_2 + O_2$$

where $O(^3P)$ is atomic oxygen in ground state and M is either N_2 or O_2.

This results in O_3 in a photostationary state and its formation are dictated by the NO_2 photolysis rate and the $[NO_2]/[NO]$ ratio. When VOCs are present, they react to form radicals which either consume NO or convert NO to NO_2, which, because of the photostationary state relationship, causes O_3 to increase. Although many types of reactions are involved, the major processes can be summarized as follows:

$$VOC + OH \rightarrow RO_2 + products$$

$$RO_2 + NO \rightarrow NO_2 + radicals$$

$$Radicals \rightarrow OH + products$$

The rate of ozone increase caused by these processes is dependent on the amount of VOCs present, the rate constants for the VOCs initial reactions, and the level of OH radicals and other species with which the VOCs might react.

CO is also one of the major ozone precursors other than VOCs. The enhancement of CO in the lower atmosphere will have the possible interaction of the CO-OH-CH_4 cycle that affect the partition between NO_x and HNO_3 and other key ratios of radicals species. The high CO concentration level will create the interaction of the CO-OH-CH_4 (Sze, 1977) cycle shifting OH into HO_2 (i.e. elevating HO_2 relative to OH via the cycle). The reaction of HO_2 with NO followed by photolysis of NO_2 will produce atomic oxygen, which readily combines with molecular oxygen to form ozone (Liu et al., 1987). Also note that suppression of OH by high CO will elevate or free-up more NOx, because of lesser OH for converting NO_2 into more inert form HNO_3. One possible ozone production sequence can be written as:

$$CO + OH \rightarrow CO_2 + H$$

$$H + O_2 + M \rightarrow HO_2 + M$$

$$HO_2 + NO \rightarrow OH + NO_2$$

$$NO_2 + hv \rightarrow NO + O$$

$$O + O_2 + M \rightarrow O_3 + M$$

$$\text{Net: } CO + 2O_2 \rightarrow CO_2 + O_3$$

Eventually, this chemical mechanism may lead to the formation of ozone during the long range transportation process.

2.6. Reviews of air pollution transport in South China region

2.6.1. Air pollution transport within boundary layer

Situated on the coast between the Asian continent and the South China Sea, the cities in South China region are under the strong influence of the summer and winter Asian monsoons. Chan et al. (1998) reported with surface O_3 measurements that surface O_3 in Hong Kong had an autumn maximum and summer minimum. The seasonal alternation of the prevailing oceanic and continental air masses, plus the climate system associated with the Asian monsoon system, were the governing factors for the temporal O_3 pattern. The aged air masses associated with the continental outflow from China carried with their anthropogenic air pollutants to the downwind areas. Under favorable meteorological conditions for photochemical O_3 formation in southeast China, the O_3 level reached a maximum in autumn. In contrast, the occurrence of the O_3 summer trough was due to the inflow of clean oceanic air masses by the summer monsoon.

Thailand is situated at the tropical region of continental parts of Southeast Asia. Pochanart et al. (2001) reported the surface O_3 observation at two rural/remote sites in Thailand during 1996 to 1998. The study revealed the basic picture of surface O_3 characteristics in Thailand. The seasonal variations of ozone showed dry season maximum-wet season minimum characteristics. The variations were controlled primarily by the long-range transport of ozone under the Asian monsoon which was the typical O_3 characteristics in the continental parts of tropical Southeast Asia. The trajectory analysis suggested that the O_3 mixing ratio associated with the

long-range transport of clean marine air mass from the Indian Ocean during the summer monsoon or wet season was as low as 13 ppb on average. During winter monsoon or dry season, the O_3 mixing ratios associated with long-range transport of continental air mass from the Asian continent showed high concentrations from 26-42 ppb for NE and W/NW air masses. The very high ozone episode observed during the local summer of the dry season was believed to be caused by the local/sub-regional scale biomass burning in Southeast Asia.

Meteorology plays an important role on the air pollution transport. On average, about 24 tropical cyclones develop over the western Pacific and the China Seas each year. Of these about six may come within 400 nautical miles of Hong Kong. Wang and Kwok (2003) analyzed a photochemical episode in September of 2001 in the Pearl River Delta (PRD). High concentrations (>120 ppbv) of O_3 were observed at a rural coastal site in western Hong Kong for six consecutive days, when a tropical cyclone, Nari, approached to Hong Kong from East China Sea. During the episode, fewer clouds were observed due to the result of heating in the large-scale descending air mass occurring at the outskirts of the low pressure system. As a result, favorable conditions with high temperature and clear sky were provided for the O_3 photochemical formation and buildup. In addition, under the influence of the counterclockwise flow around the low pressure system, the urban plumes with high concentrations of primary pollutants were brought to Hong Kong by the north-northeast land breezes.

2.6.2. Air pollution transport in free troposphere

In the lower free troposphere over South China, Chan et al. (2003a) performed the ozonesonde launching experiments to show that the O_3 enhancement over the lower troposphere were caused by SE Asian biomass burning emissions. Biomass burning emissions in the tropics had been reported to exert a strong influence on the abundance of trace gases in the atmosphere (Crutzen and Andreae, 1990). Christopher and Kimberly (1996) had successfully identified east-central India and the region containing Thailand, Laos, Cambodia and Vietnam as the two major areas of biomass burning in India and Southeast Asia. Large amounts of carbon monoxide, hydrocarbons and nitrogen oxides are emitted to the atmosphere and were transported downwind. VOCs are known to be ozone precursors (Carter, 1994). The secondary pollutant, ozone, was formed through the photochemical reactions when there were sufficient oxides of nitrogen (NOx) and ultra violet light as described in section 2.5.

Recently, ozone enhancements in the middle troposphere over South China were found to relate to biomass burning of land scavenging or accidental forest fire from the tropical and subtropical region of SE Asia. The air masses from these kinds of burnings always contain high water vapor content. During winter and early spring, agricultural and land clearing burnings take place over northern Indochina of the tropical SE Asian continent and the burning emissions were observed to be transported by the westerly towards South China. It had been shown to have a marked influence on the ozone enhancement over Hong Kong (Liu et al., 1999; Chan et al., 2003a). Chan et al. (2000) found that such air masses with ozone

enhancements carried high water content. Chan et al. (2001) also showed that the large-scale 1997 Indonesian forest fires caused an enhancement of tropospheric ozone and additional radiative forcing on a regional scale.

One of the interesting questions about the large-scale forest fires and biomass burnings is how the climate system responds to the emission of these open burnings and the associated ozone enhancement. Changes in the distribution and amount of ozone in the troposphere are expected to affect the surface-troposphere system through spatial and temporal changes in the flux of radiative energy into and out the system (Granier et al., 1999). The quantity is defined as the response in the net radiative energy flux at the tropopause to the changes in the concentration of a radiative gas. The surface temperature changes (ΔT) for a given change in radiative forcing (ΔF) can be defined by the following relationship (Masters, 1998; Granier et al., 1999):

$$(\Delta T)=f\,(\Delta F)$$

where f is the climate sensitivity parameter. This parameter depends on how much the outgoing radiant energy at the top of the atmosphere changes as the surface temperature changes. Chan et al. (2001) estimated the radiative forcing F and surface temperature change due to ozone enhancement over the Hong Kong region by the effect of the 1997 Indonesian forest fires. They revealed that there may have been an extra of 0.21 and 0.44 W m^{-2} added to the normal forcing, which induced increases of surface temperature by 0.12^{o} and 0.24^{o}C, respectively on 16 October and 3 December 3, 1997, during the period of 1997 Indonesian forest fires.

Other than the biomass burnings in SE Asia, abnormal crude oil open burning is also one of the major sources of emission on a global scale in comparison to other sources, such as mobile and industrial sources. More than 800 oil wells were ignited and more than 650 of them were in flames for several months during the Gulf War in 1991. As a result, smoke plumes from the burning oil wells reduced the solar radiation by 26-36% in Jubail, Saudi Arabia during the period January-June 1991 (Bahrain Meteorological office, 1993). Even in East Asia, which is located far away from the Persian Gulf, black snow was observed for a week during 20-25 February, 1991 at Matsue, Shimane Prefecture in Japan (Tazaki et al., 1992). When we just began to forget the Gulf War, the Iraq War started on 21 March, 2003. Although the war quickly ended in May 2003, terrorist attacks by the extremist groups were reported every few days. The oil pipeline network systems were frequently sabotaged (Geotimes December, 2004). Significant emissions of ozone precursors are found to transport downwind by the westerly wind as a result of the crude oil burnings. During the TAPTO-China experimental period in spring of 2004, Wong et al. (2006) performed the ozonesonde field measurements launching on three sites of South China at Tengchong in Yunan Province, Sanya in Hainan Province and Hong Kong in the southwest of Guangdong Province. High O_3 mixing ratios were concurrently observed in the middle troposphere at these three launching stations during the news of oil field fires in Middle East reported at the beginning of May in 2004. By examining the satellite data, abnormal fire hot spots were also observed at the beginning of May in 2004 in Persian Gulf region. The emissions from these crude oil burnings were supported by high concentration of CO column

from the Measurements of Pollution in the Troposphere (MOPITT) satellite and high value of aerosols index (AI) from the TOMS absorbing AI product in this region. The ozone rich air masses detected in the middle troposphere in South China were attributed to the crude oil open burning.

One may consider that the ozone intrusion from stratosphere to troposphere may be the sources of ozone enhancement in upper and middle troposphere in SE Aisa. Therefore, during the Transport and Chemical Envolution Over the Pacific (TRACE-P) period in the spring of 2001, Chan et al. (2003a) launched ozonesonde at three Chinese sites: Kumming in Yunan Province, Hong Kong in the southeastern coast of Guangdong Province, and Linan in the Hangzhou Province. The sites extend from subtropical southwestern China close to the Southeast (SE) Asian border, to the southeastern Asian coast, and to the edge of the middle latitudes of central eastern China, respectively. The results showed that there were substantial variations in the vertical O_3 distributions over these sites. There were high O_3 values in the middle and upper troposphere of Linan, and frequent O_3 enhancements in the lower troposphere of Hong Kong and Kumming. Stratospheric ozone intrusion is one of the major sources of ozone enhancement in the upper and middle troposphere in Northeast Asia (Murao et al., 1990; Austin and Midley, 1994; Tsutumi et al., 1994; Sunwoo et al., 1994). Linan is located at the edge of the subtropics close to the mid-latitude. Stratospheric O_3 was found to be the major contributing source to middle and upper tropospheric O_3 in Linan. In contrast, since Hong Kong and Kumming were situated in the subtropical regions and were relatively far away from the jet stream, the contributions of stratospheric O_3 to tropospheric O_3 were relatively low.

Potential vorticity (PV) is a dynamic tracer of stratospheric air in the troposphere (Danielsen, 1968). The finding was supported by the poor relationship between O_3 and PV.

2.7. Reviews of air pollution transport in Northeast China region

2.7.1. Air pollution transport within boundary layer

In the fast developing Yangtze Delta region of China, Wang et al. (2001) presented the measurements of O_3 and primary pollutants at a rural site Linan in Hangzhou Province, China. Results indicated that the primary pollutants (CO, SO_2, and NOx) are high in winter and low in summer in Northeast Asia. The winter peaks are believed to be due to a higher energy demand (for heating), slower chemical destruction rates, and weaker vertical mixing, as well as the transport of urban/industrial emissions from the Shanghai metropolitan area (by prevailing northeasterly winds) in winter. This study also suggested that photochemically produced ozone is linearly dependent on NOx.

Surface O_3 and CO measurements were performed at Oki Island, Japan, by Pochanart et al. (1999) from 1994 to 1996. The analyses were based on isentropic trajectories. The O_3 and CO characteristics in this region were controlled by the long-range transport of continent and marine air masses driven by the Asian monsoon regime and photochemical activity due to anthropogenic sources on a regional scale. The continental background air mass, defined from those originating in east Siberia and passing over the regions free from anthropogenic sources to reach Oki, showed seasonal cycles of O_3 and CO with spring maximum and summer minimum. The regionally polluted continental air mass, influenced by the intense anthropogenic activities in northeast Asia during transport, showed spring-summer board maximum and winter minimum of O_3. Comparison of the air mass categorized

O_3 data at Oki Island with the selected sites in Europe had revealed a similar seasonal variation pattern but with higher concentration levels at Oki Island, which probably reflected less photochemical activity and the inflow of Atlantic marine air in Europe.

Large-scale forest fire is one of the major sources of air pollution in Northeast Asia. Although most forest fires occur in tropical areas, major fires have also occurred at high latitudes (Cahoon et al., 1994; Duncan et al., 2003). Boreal ecosystems are mostly occupied by forest that wraps around the Northern Hemisphere's circumpolar regions covering about 1.4 x 10^9 ha and forest fire is therefore one of the major sources of air pollution in Northeast Asia. One of the major forest fires in Northern Hemisphere is Boreal forest fires. Boreal forest fires are unique in comparison to other forest fires in their variety of causes, severity, and amount of ground layer burning (Kasischke and Stocks, 2000). Anthropogenic activities are a major cause of Boreal forest fires. It has been estimated that 86.3% of all fires in Russia during the last 3 decades were caused by human activity (Shvidenko and Nilsson, 2000); natural factors, usually lightning, caused 10 – 15% of the fires. However, the impact of such fires on the atmosphere in boreal forests remains largely unknown due to the lack of exact source information.

Boreal forest fires tend to spread quickly, so a large boreal fire releases enough thermal energy to create smoke and convection columns that extend into troposphere and sometimes to the tropopause and even stratosphere (Cofer et al., 1996; Fromm et al., 2000). Recently, extensive fire activities occurred during early summer in 2003 around the Siberian border in Russia between Amur and Lena rivers.

Lee et al. (2005) analyzed the satellite data and ground-based measurements to show that the 2003 Siberian forest fire had adverse effects on the regional air quality and radiation budget in Korea. Smoke pollution plumes from these kind of Russian forest fires were often found to transport to Northeast Asia, through Mongolia, Northeastern China and Korea.

2.7.2. Air pollution transport in free troposphere

Stratospheric ozone intrusion is among the major sources of tropospheric ozone enhancement in Northeast Asia including Northeast China. In East Asia over Japan, the springtime tropospheric O_3 enhancement is explained by intrusion of stratospheric O_3 into the troposphere and is linked to the meteorological phenomenon associated with the East Asia jet stream (Murao et al., 1990; Austin and Midley, 1994; Tsutumi et al., 1994; Sunwoo et al., 1994). These phenomena include tropopause folds, cut-off lows and streamer along jet stream. The East Asia jet over the East Asia coast, including eastern China, is the largest jet stream in the world in spring (Ding, 1994). It comprises of a subtropical jet and is linked to the presence of a semi-permanent pressure trough over the Asian continent and a large temperature contrast at the East Asia coast. Such large scale perturbations in the flow penetrate into the westerly winds in the stratosphere and affect the distribution of O_3 available for transfer into the troposphere during spring (Austin and Midgley, 1994). Chan et al. (2003b) measured the troposheric O_3 profile over the east China coast at Linan by electrochemical concentration cell ozonesondes in the spring of 2001. They used potential vorticity (PV) and meteorological analyses to trace the

origins and sources of O_3. The analysis revealed that the stratospheric O_3 is the predominant source of O_3 in the middle and upper troposphere, while anthropogenic sources caused high O_3 pollution episodes in the boundary layer.

Crude oil burning is among the major types of open burnings in Middle East and Japan is located to the central latitude of Far East Asia. However, Tazaki et al. (2004) reported that the low pH value of rain and high value of electrical conductivity (EC) in the rainwater were caused by the oil field fires in Middle East even they are about 8000 km apart. Since 21 March, 2003, the Iraq plunged into the war and 9 oil field fires were reported on 25 March, 2003, in Rumaylah oil field near the borderline of Kuwait. Once the oil fields get fired, it takes several months to extinguish the fire and the black carbon particles were produced due to incomplete combustion. These particles were then blown up to the middle troposphere by the hot wind in desert. In the meantime, Oltmans et al. (2004) calculated the climatological wind fields for the period 1991-2001 over the North Pacific at the middle troposphere at 500 hpa. Westerly wind was found to be the prevailing wind in spring from March to May. Thus, the emissions from the Middle East could be transported downwind to East Asian Japan even they are far apart. The effects of the oil field fires in Iraq's War to the atmosphere in Japan were also supported by the detection of contamination of depleted Uranium (DU) from Iraq's War.

2.8. Historical review inferred further scientific interests

China has a land area of 9.6 million km^2, occupying 6.5 percent of the total land area of the world. The distance is 4500 km measured from west to east direction and 4200 km measured from north to south direction. Thus, China has a geographical location for temperate and subtropical climates. With regard to the climate of China, the impact of air pollution will not only be applied to China itself, but also to the whole Asia-Pacific region. Meteorology plays an important role on the transport of air pollution. Recently studies have shown that the emissions from China may have significant effects on tropospheric chemistry and the biogeochemical cycles of the remote Pacific (Crawford et al., 1997; Elliott et al. 1997).

My study comprised two phases of experiment and these two experiments described in chapter 1 were all performed in springtime. It is because the March-May timing corresponds to the transition from the winter to the summer monsoon over Asia. As the season progresses from winter to spring, convection becomes significant and tends to mix pollution from the west and carried along by the westerly wind (Jacob et al., 2003). At the same time, spring is the dry season in Asia. This season is favorable for the occurrence of forest fire (Dwyer et al., 1988, Christopher et al., 1998). In late winter and early spring, people in the Asian subcontinent starts to burn their crop residues of prior year making preparation for cultivating next crops by setting out fires. These human initiated fires very often become out of control and trigger larger scale forest fires in Asia.

The historical review of air pollution transport in Southern and Northern Asia has inferred further scientific interests which lead to the past study. The following chapters will give an overview of the experiments performed.

CHAPTER 3 – EXPERIMENTAL SETUP, SAMPLING AND ANALYSIS METHODOLOGY

3.1 Introduction

My study comprised two phases of experiment. During the first phase study in spring of 2004, surface O_3 and CO and aerosols over the Tibetan Plateau were measured at the southwestern border of China. While in the same period in the spring of 2005, surface O_3 and CO were measured at the rural site in Northeast China. A detailed description of the sampling sites will be presented in this chapter. The measuring technique and chemical analysis will also be discussed. The satellite data used in this study will be described.

3.2. Field measurements in Tengchong County, Yunan Province

3.2.1. Sampling site description

Tengchong (25.01^{o}N, 98.3^{o}E) is situated on the eastern edge of the Tibetan Plateau, with an average altitude of 1640 m a.s.l. It is located 60 km to the east of the Myanmar border and 750 km to the west of Kunming, the capital of Yunan province (Figure 3.2.). The monitoring station is situated on the top of a mountain at Tengchong Background Meteorological Station (Figure 3.1.), with an altitude of 1960 m a.s.l. It is located 5 km to the south of the ozonesonde launching station. There are small hills and a few small villages surrounding the station. The hills are planted with different types of trees and crops. It is a remote and rural area typical of the relatively undeveloped western part of China.

3.2.2. Equipment setup for the ground-based measurements

Surface O_3, CO, PM_{10} and $PM_{2.5}$ were continuously measured from 7 April to 24 May, 2004. The instruments were housed in a temperature-controlled laboratory. Ambient air samples were drawn through a PFA Teflon tube with a 3/8" inside diameter. The sampling inlet was located 3 meters above the ground level on the rooftop of the station. The other end of the sampling line was connected to a glass-made buffer and a bypass pump drawing air at a rate of 10 l/min. The intakes of the analyzers for O_3 and CO were connected to the buffer. The aerosol analyzers were connected to the inlet funnel by a tygon extension line of ½ inch inside diameter and 0.5 m long.

One portable air sampler (MINIVOL, AIRMETRICS, USA) was setup for collection of air particles for further chemical analysis in the sampling period. It was placed on the rooftop of the station which was 3 meters about the ground level. During sampling, air is drawn through a particle size separator with PM_{10} cut point and then through a 47 mm Whatman quartz microfibre filter (QM/A) which collects the particles in the air stream. The filters were pre-heated at 800^{o}C for 3 h before use and were placed in clean polyethylene Petri dishes and wrapped with Teflon tape before and after field measurement. The sampling duration was 24 h.

Figure 3.1. Picture of Tengchong Background Meteorological Station

3.3. Field measurements in Long Fengshan Station, Heilongjiang Province

3.3.1. Sampling site description

The study was conducted at the Long Fengshan World Meteorological Organization (WMO) Regional Background Station (44°44'N, 127°36'E, 330.5 m asl), which is one of the four WMO Regional Background Stations in China (Figure 3.2.). It is situated in a forest within Heilongjiang Province and distant from major population and industrial centers (Figure 3.3.). The closer sources of anthropogenic emissions to the Long Fengshan site are Jinlin about 130 km to the south-southwest and Changchun about 210 km to the southwest. The population of Heilongjiang Province was 38.27 million in 2005.

3.3.2. Equipment setup for the ground-based measurements

Surface O_3 and CO were continuously measured from 1 April to 15 May, 2005. The instruments were housed in a temperature-controlled laboratory. Ambient air samples were drawn through a PFA Teflon tube with a 3/8" inside diameter. The sampling inlet was located 3 meters above ground level on the rooftop of the station. The other end of the sampling line was connected to a glass buffer and a bypass pump drawing air at a rate of 10 l/min. The intakes of the analyzers for O_3 and CO were connected to the buffer.

3.3.3. Non-methane hydrocarbons sampling

Air samples were collected at the rooftop of Long Fengshan WMO station using pre-evacuated 2-L stainless steel canisters provided by University of California, Irvine (UCI). A flow restricting tube was installed at the inlet of each canister to control the sampling flow rate to 35 ml/min and the sampling duration was kept for about one hour. Samples were collected between 14:00-15:00 once every second day. Additional samples were collected during the intensive study period from 14-22 April, in which one sample was collected between 14:00-15:00 each day. There were totally 24 air samples from 1 April – 15 May. The canisters were then sent to the Research Center for Environmental Changes, Academia Sinica, Taiwan for further analysis.

Figure 3.2. Map showing the location of sampling sites in this study

Figure 3.2.Picture of Long Fengshan WMO Regional Background Station in Heilongjiang Province

3.4. Measurement Technique

Surface O_3 concentration was measured by a 2B Technologies O_3 Monitor, which works on the principle of absorption of ultraviolet light at 254nm by O_3 molecules. The analyzer incorporates corrections due to changes in temperature and pressure in the absorption cell and drift in the intensity of the UV lamp. The detection limit of the analyzer is 1.5 ppb. CO was measured by an Advanced Pollution Instrumentation, Inc. (API), non-dispersive infrared Model 300E analyzer. The detection limit is about 40 ppb for a 5-min average. The analyzers were calibrated before and after the field study by an API dynamic dilution calibrator (Model 700) and standard gases traceable to NIST standards. No significant change in the responses of the analyzers was seen before and after the observation. The possible baseline drifts of the analyzers were checked on a frequency of per day by standard zero air generated by the calibrator and with the help of an O_3 scrubber supplied by the manufacturer. For the O_3 analyzer, zeroing lasted for 15 minutes. The last 5-min data for each zeroing was taken as the baseline.

The real-time $PM_{2.5}$ and PM_{10} concentrations were measured by portable monitors (DustTrak, TSI Model 8520). The monitor works under the laser photometer principle with light scattering technique and in the range of 0.001-100 mg/m^3 (calibrated to respirable fraction of standard ISO 12103-1, A1 test dust). It measures particles size ranging from 0.1 to approximately 10 μm (Upper limit is dependent on flow rate). The sampling flow rate is 1.7 L per minute. The concentrations of PM with aerosol diameter less than 2.5 μm and 10 μm ($PM_{2.5}$ and PM_{10}) are distinguished by an impactor installed in the inlet of the monitor. The

monitors were calibrated against standard gravimetric samplers (Tapered Element Oscillating Microbalance, TEOM, 1400a) that are specified in the Federal Reference Method (FRM) before deploying the instruments for observation. The MINIVOL sampler was also subjected to a parallel comparison against standard gravimetric sampler (TEOM, 1400a) before the field study. The relative deviations of the measured concentrations were within 5%. Comparison of the daily $PM_{2.5}$ and PM_{10} concentrations measured by TEOM, Mini-volume and DustTrak samplers were shown in Figure 3.4.

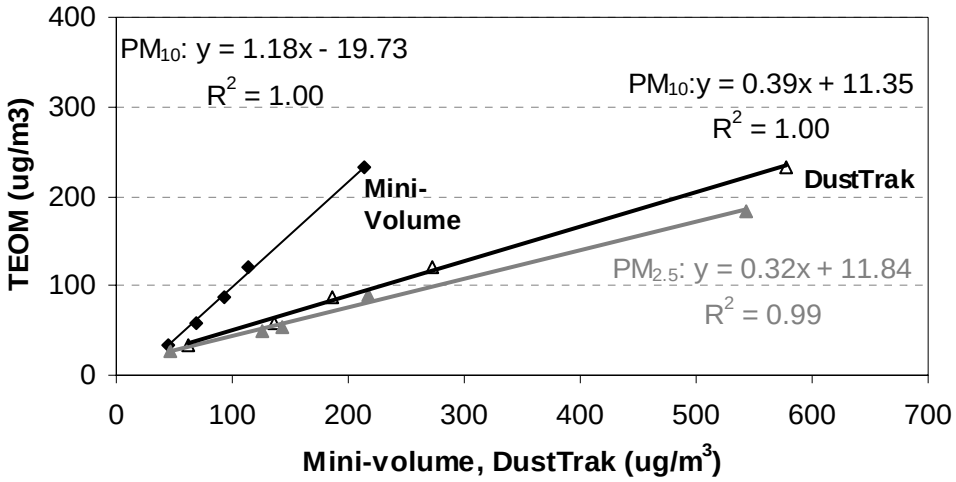

Figure 3.4. Comparison of the daily $PM_{2.5}$ and PM_{10} concentrations measured by TEOM, and Mini-volume and DustTrak samplers.

3.5. Analysis of water-soluble inorganic ions

The loaded filter samples in the spring of 2004 were then sent back to the laboratory of The Hong Kong Polytechnic University (HKPU) for the chemical analysis of water soluble inorganic ions. The filters were digested using a laboratory microwave extraction system to extract metals with a hydrochloric/nitric acid solution (USEPA Methods IO 3.1). The digestate was filtered and then diluted to 25ml with distilled-deionized water. All the filters were extracted using ultra-pure water. The extraction solutions were filtered and stored in plastic vials in the refrigerator at 4^{o}C until chemical analysis. Chemical analysis of the water-soluble inorganic ions was determined by using the ion chromatography (DIONEX ICS 2500). The detection limit and uncertainty for potassium ion were 0.003μg/$m^3$and 6% respectively.

3.6. Experimental methods for the analysis of NMHCs

Air samples during the 2005 field measurements were collected in 2-liter stainless steel canisters (provided by University of California, Irvine). All canisters were evacuated and humidified prior to sample collection. An automated GC/MS/FID (Varian 3800 and Saturn 2000) system designed for air analysis was used to analyze C_2–C_{10} VOCs in all of the air samples. Two capillary columns, a PLOT (Chrompack; 50m x 0.32 mm; d_f = 5:0 µm) and a DB-1 (J&W; 60m x 0.32 mm; d_f = 1:0 µm), were connected in parallel by a Y-splitter with 1/3 flow entering the PLOT column. The PLOT column connected to flame ionization detection (FID) was responsible for separation and detection of C_2–C_4 compounds, and the DB-1 column was connected to the MS for separation and detection of C_4–C_{10} compounds. The scan range of MS was m/z 10–180. 56 hydrocarbon species were quantified from each injection. Four internal standards (bromochloromethane, 1,4-difluorobenzene, chlorobenzene- d5, and 1-bromo-4-fluorobenzene) were blended in for each injection aliquot to confirm the stability of MS and to ensure data quality.

Each aliquot of 190 ml from the canisters was drawn to the cryogenic trap packed with fine glass beads cooled at -170^{o}C for pre-concentration. Note that drawing more than 190 ml air from the canister could end up plugging the trap by water. During injection, the trap was resistively heated up to 80^{o}C within seconds, and a stream of high purity He flushed the trapped VOCs onto the columns. The oven temperature was initially held at -50^{o}C for 3.1 min, then ramped to -10^{o}C at 20^{o}C/min, to 120^{o}C at 5^{o}C/min, to 180^{o}C at 20^{o}C/min, and held at 180^{o}C for 21.5 min. 2.2.

3.7. Analytical method used in this study

3.7.1 Satellite images of fire count

We used the fire maps of the SE Asian and Russian regions of the University of Maryland to identify biomass-burning activity in SE Asian and NE Asian regions (http://maps.geog.umd.edu/products.asp). The fire maps show the spatial distribution of fire spots detected by the MODIS (Moderate Resolution Imaging Spectroradiometer) Rapid Response System using a standard MODIS MOD14 Fire and Thermal Anomalies Product algorithm. The fire map is generated from MODIS Web Fire Mapper which is developed by the maps of active fires detected by the Terra and Aqua MODIS instruments. MOD 14 fire product can identify the active fires and other thermal anomalies, such as volcanoes. The individual detection on the map represents the centre of a 1 km pixel containing at least a fire within that pixel.

3.7.2 Datasets used to estimate the synoptic weather conditions

In order to estimate the synoptic weather conditions, the global gridded final run (FNL) meteorological data were used to calculate the surface wind field and plot the pressure chat over the study area. FNL data, which uses the Global Spectral Medium-Range Forest model to assimilate multiple sources of measured data and forecast meteorology, are available from the National Oceanic and Atmospheric Administration (NOAA) Air Resource Laboratory. Backward trajectory of air mass were calculated from the Hybrid Single-Particle Lagrangian Integrated Trajectory (HYSPLIT-4; Draxler and Hess, 1997) model.

HYSPLIT model is the newest version of a complete system for computing simple air parcel trajectories to complex dispersion and deposition simulations. It has improved advection algorithms, updated stability and dispersion equations, a new graphical user interface, and the option to include modules for chemical transformations.

HYSPLIT_4 is designed to support a wide range of simulations related to the long-range transport, dispersion, and deposition of pollutants. The applications can range from the need to respond to atmospheric emergencies, ranging in character from accidental radiological releases to the hazards presented to aircraft operations from volcanic ash eruptions, or routine air quality assessments such as those associated with emissions of anthropogenic pollutants. Simulation output results can vary from simple trajectories to more complex air concentration contour patterns. Calculations can be performed on archive or forecast meteorological data, or a combination of both.

The dispersion of a pollutant is calculated by assuming either puff or particle dispersion. In the puff model, puffs expand until they exceed the size of the meteorological grid cell (either horizontally or vertically) and then split into several new puffs, each with its share of the pollutant mass. In the particle model, a fixed number of initial particles are adverted about the model domain by the mean wind field and a turbulent component. The model's default configuration assumes a puff distribution in the horizontal and particle dispersion in the vertical direction. In this way, the greater accuracy of the vertical dispersion parameterization of the particle

model is combined with the advantage of having an ever expanding number of particles to represent the pollutant distribution.

In most circumstances the input meteorological data will contain a vertical motion field, usually in pressure units, and regardless upon which vertical coordinate system these input data are provided, the vertical velocity field is always relative to the metrological model's native terrain-following sigma coordinate system. The trajectory and dispersion model calculations can use these data fields directly because the model's internal coordinate system will always be terrain following regardless of the form of the input data. This is one of the primary reasons that the input data need to be remapped to a common vertical coordinate system.

The HYSPLIT model can run multiple nested input data grids and is linked to Air Resources Laboratory (ARL) and National Weather Service's National Centers for Environmental Prediction (NCEP) meteorological data server. The meteorological data that are an optional output with each trajectory are valid at that trajectory position and time as interpolated from the meteorological data file used for the trajectory calculation. The values come from NOAA's NCEP meteorological models, run at either 12 km (ETA) or 100 km (GFS) resolution. However, these data are interpolated to grids at coarser resolution that we use for transport and dispersion calculations. They may not be representative of a nearby measurement. That will depend upon local effects as well as the larger scale gradients of the variable and how well a gridded field can represent a continuous function.

In order to investigate the influence of large-scale motion of air masses on the characteristics of O_3 and other trace gases and aerosols in this region, 3-D

backward air trajectories calculated by (NOAA) HYSPLIT Model were used to determine the source region of air masses (Draxler and Rolph, 2003; Rolph, 2003). The input data of the model is from the National Centre of Environmental Prediction (NECP)'s Global Data Assimilation system. Air-mass backward trajectory calculations were made using the isentropic method. The data has a time resolution of 6 hr, horizontal resolution of 1 degree.

3.7.3. TOMS aerosol index

TOMS (Total Ozone Mapping Spectrometer) absorbing aerosol index data (Herman et al., 1997) from the NASA/Goddard Space Flight Center (http://toms.gsfc.nasa.gov) were used to estimate smoke aerosol generated by the Korean forest fire in NE Asia. The TOMS AI product has been used to detect UV absorbing aerosol, including biomass-burning aerosols. The TOMS AI is defined as the difference between the observations and model calculations from a pure molecular atmosphere with the same surface reflectivity and measurement conditions (Hsu et al., 1996; Herman et al., 1997). Generally, positive AI values reflect the presence of absorbing aerosols; the presence of non-absorbing aerosols will suppress the AI value. TOMS AI data were used in this study to calculate the effect of Korean forest fire on Northeast China to confirm the aerosol plumes from Korean peninsula. A TOMS AI map provides the magnitude and duration of smoke aerosol, which vary temporally over the study area.

CHAPTER 4 - EFFECTS OF SOUTHEAST ASIAN FIRE ACTIVITIES ON TRACE GASES AND AEROSOLS OVER THE TIBETAN PLATEAU OF SOUTHWEST CHINA IN THE SPRING OF 2004

4.1. Introduction

The widespread air pollution in South and Southeast (SE) Asia, and China is a subject of scientific interest and public concern. In South and SE Asia, forest fires, burning of biomass/biofuels (e.g. wood, dung and agricultural residue) are major sources of air pollutants (UNEP and C4, 2002). The Tibetan Plateau is the largest plateau in the world that exerts profound thermal and dynamic influences on local and global climate, and atmospheric circulation of the Asian Monsoon System. Each March and April, an air mass starts to inflow from the Indian Ocean through the Bay of Bengal and the Tibetan Plateau towards inland Asia. The water content, physical and chemical properties of the air mass have vital regional influences on the weather and climate of China and East Asia.

However, field data of trace gases and aerosols that are chemically and radiatively important for the Tibetan Plateau are scarce .In my study, surface O_3 and its precursors (CO) and aerosols over the Tibetan Plateau were measured at the southwestern border of China in spring of 2004. In this study, the results were presented and analyzed with an emphasis on the impact of the biomass-burning emissions, as the result of fires in SE Asia and pollution from South Asia, on surface O_3, trace gases and aerosols over the Tibetan Plateau of Southwest China.

4.2. Concentration levels of O_3, CO and aerosols

Figure 4.1 shows the daily average concentrations of O_3, CO, aerosols and rainfall. Table 4.1 summaries their statistics. Ozone, CO, $PM_{2.5}$ and PM_{10} had average hourly concentrations of 26 ppb, 179 ppb, 28 and 34 μg/m^3, respectively. They exhibited large variations during the experimental period with lower values at the beginning and the end of the experimental period, and gradual increases in between until they, except CO, reached maximum daily averages of 47 ppb for O_3, 79 and 95 μg/m^3 for $PM_{2.5}$ and PM_{10}, respectively, from 6 to 10 May. The maximum daily average of CO in this period was 287 ppb. The highest daily CO concentrations, 245-308 ppb, were found from 24 to 30 April, when other species also showed high values.

Table 4.1. Measurement statistics of ozone, CO and aerosols during the spring of 2004

	Concentrations					
	Mean	Stdev.	Min.	Max.	75%	25%
O_3 (ppb)	26	8	9	59	31	20
CO (ppb)	179	91	23	678	224	113
PM_{10} (μg/m^3)	34	23	0	158	46	17
$PM_{2.5}$ (μg/m^3)	28	19	0	137	36	14

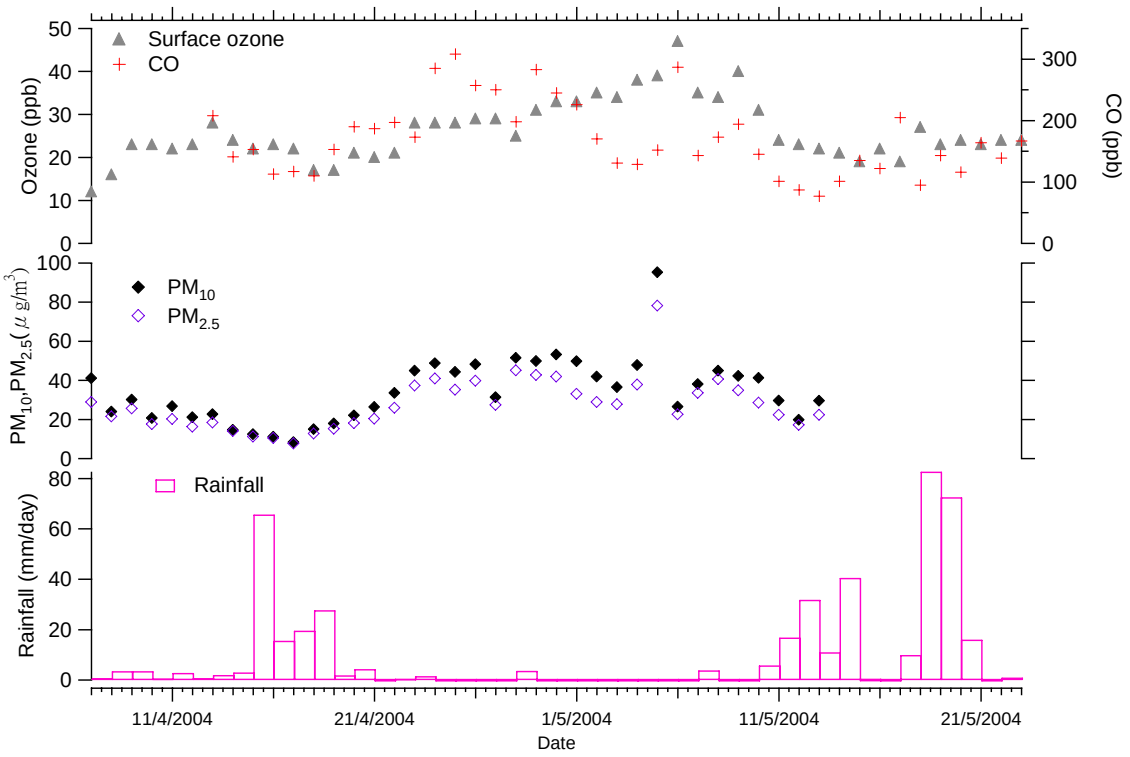

Figure 4.1. Daily average concentrations of O_3, CO, PM_{10}, $PM_{2.5}$ and rainfall during the spring of 2004.

4.3. Diurnal variation of O_3, CO and aerosols

The averaged surface O_3 exhibited a minimum of ~22 ppb in the morning (6:00) and gradually increases afterwards until it reached a maximum of ~31 ppb in the early afternoon (14:00) (Figure 4.2). It was then followed by a gradual decrease until next morning. CO and aerosols showed a more obvious bimodal pattern with a major peak at late night hours (21:00–22:00) and a minor peak in the morning (8:00–9:00). They showed lower values in the afternoon (15:00–16:00). The daytime increase in O_3 concentration was due to the photochemical O_3 formation from its precursors such as CO, methane and non-methane hydrocarbons in the presence of NOx and sunlight. The O_3 decrease after the sunset was due to the fact that there was no O_3 being produced and an increase of dry deposition of O_3 in a shallow boundary layer as a result of the radiative cooling of the underlying ground surface, which also caused an accumulation of CO and aerosols at night.

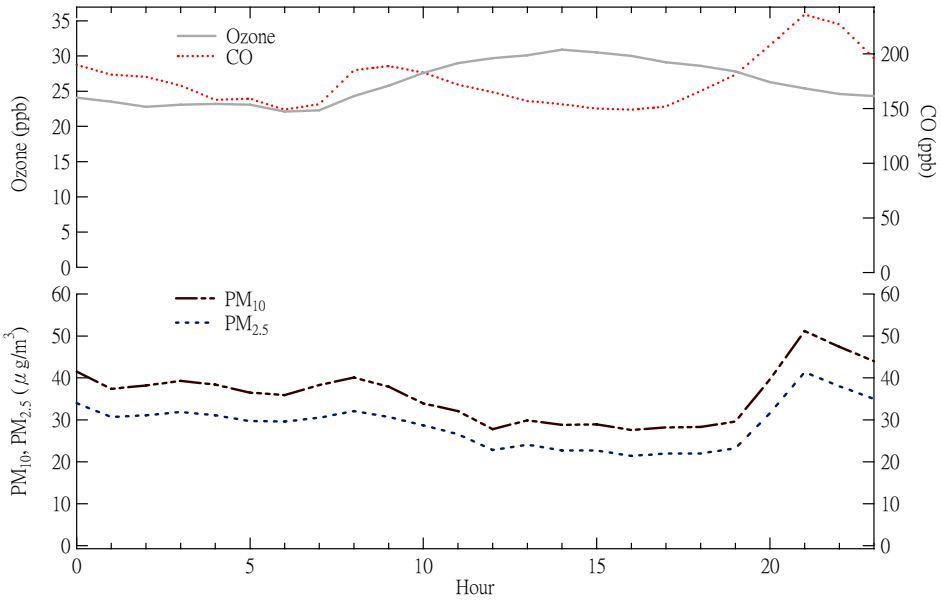

Figure 4.2. Average diurnal variations of O_3, CO, PM_{10} and $PM_{2.5}$ concentrations

4.4. Comparisons of the concentrations of O_3, CO and aerosols over the Tibetan Plateau with other studies

The springtime surface O_3, CO and aerosols levels over the Tibetan Plateau at Techgchong were low when compared with those reported for other rural and background sites in Asia in the same period of the year. Chan et al. (2002) reported surface O_3 and CO values of 30 and 300 ppb, respectively, for the subtropical South China coast within the Pearl River Delta in Hong Kong. Wang et al. (2001) found that the concentrations of O_3 and CO were about 50 and 600 ppb, respectively, on the East China coast within the Yangzhi River Delta in Linan. These comparisons suggested that the background air in Southwest China is relatively free of anthropogenic impact compared with that in East and South China. The average concentration of O_3 in Tengchong was also lower than those reported for similar longitudinal sites in tropical Inthanon (18◦33_N, 98◦3_E, 1450 m a.s.l.) and Srinajarin (14°22'N, 99°07'E, 296 m a.s.l.), Thailand and mid-latitudinal site,Waliguan (36°17'N, 100°54'E, 3810 m a.s.l.) in Northwest China. Pochanart et al. (2001) reported monthly median O_3 concentrations of 33–55 and 28–38 ppb in April and May for Inthanon and Srinajarin, respectively, where active biomass burning occurs. The monthly average O_3 concentrations in the Waliguan Global Atmospheric Watch Station usually range from 50 to 60 ppb in April and May (Tang et al., 1996). The differences in O_3 concentrations in these sites suggest that there exist complex variations of O_3 in the Tibetan Plateau and the neighbouring SE Asian region. Ozone in Tengchong showed comparable values and a similar diurnal pattern to that measured at a tropical coastal site in east India on the Bay of Bengal (Debaje

et al., 2003). The measured O_3 and CO were comparable with the mean concentrations of 35 and 125 ppb, respectively, reported for the Northern Hemispheric mid-latitude background air at Mace Head (Derwent et al., 1998) and the values reported for other background sites in the Northern Hemisphere (Oltmans and Levy II, 1994).

4.5. O_3, CO and aerosols concentrations in different air masses

The origins and transport pathways of air mass transport reaching the measurement site can be categorized into three groups based on backward air trajectories. The air masses in the first group were related to the S/SW monsoon and originated from the Bay of Bengal and its surrounding regions. They mostly traveled across Myanmar and sometimes the Myanmar–Bangladesh and Bhutan border and less frequently the northern part of Thailand and Laos before reaching Southwest China (Figure 4.3a). In the second group, the air masses traced back to the Central Asian continent. They traveled across northern India and Nepal and Myanmar before entering the border of Southwest China (Figure 4.3b). In the last group, the air masses originated from the east. They were either associated with the Northeast Asian monsoon blowing from central and northern China (Figure 4.3c) or originated from the region close to the western Pacific and the South China Sea (Fig. 4.3d). These air masses had to pass over large geographical areas of Central and South China including Yunan, Guizhou, Guangxi and Guangdong to reach the site (Figure 4.3c).

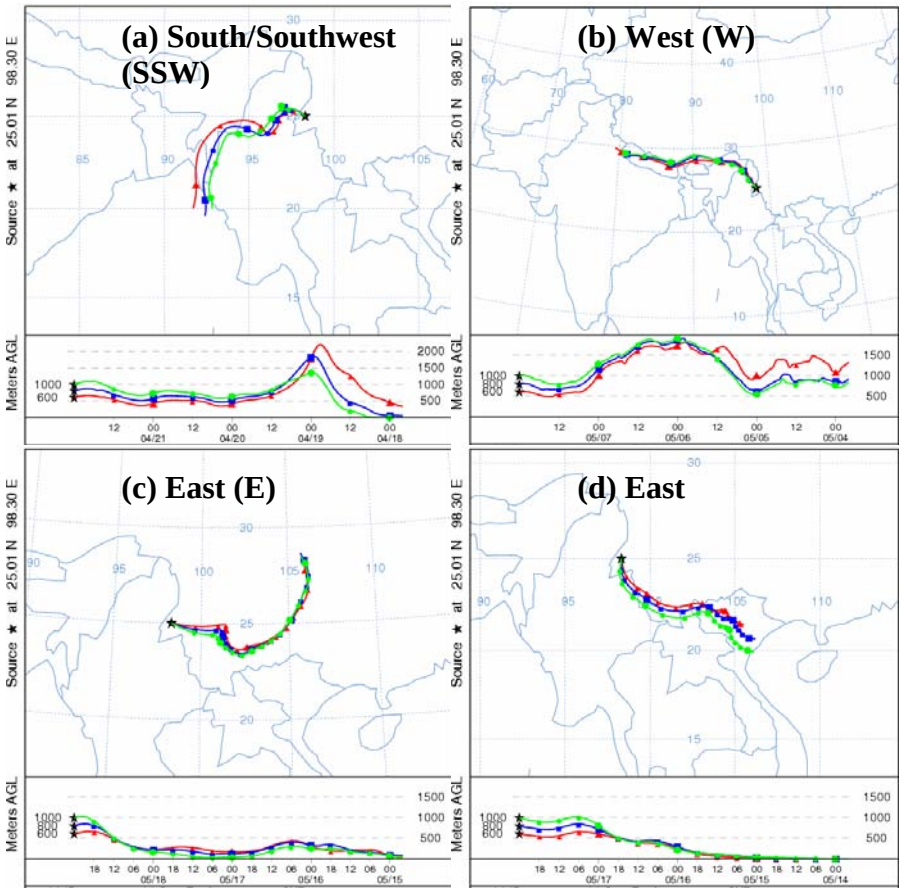

Figure 4.3. Representative air trajectories for the three air mass transport groups

Table 4.2 summarizes the surface O_3, CO, $PM_{2.5}$ and PM_{10} concentrations, daily mean temperature and daily rainfall in the three trajectory groups. The O_3, CO and aerosol concentrations associated with the western and southern air masses were higher than those in eastern air masses despite comparable daily mean rainfall in the maritime S/SW and eastern air masses. The higher levels in the S/SW air mass clearly indicated the importance of biomass-burning emissions from fire activities in the SE Asia subcontinent. This will be described in the next section. Interestingly, there was noticeably higher CO level in the continental western air masses. Ozone,

$PM_{2.5}$ and PM_{10} levels had the highest concentration in this air mass trajectory. A detailed examination of the trajectory revealed that they were due to the extensive fires occurring in the close vicinity of the western side of Yuanan province in the northern Myanmar and Bangladesh, and northeastern India region, where the air trajectories from the west had passed over (Figure 4.3). The fire activities were especially extensive during the period from 21 April to 10 May (Figure 4.4).

Table 4.2. Average concentrations (± standard deviation) of trace gases and aerosols, and meteorological parameters in the three trajectories.

	O_3	CO	PM_{10}	$PM_{2.5}$	Rainfall (mm/day)		Temperature (^oC)	
	ppb ± Stdev		$\mu g/m^3$ ± Stdev		Range	Median	Range	Mean
South/Southwest	28±8	161±64	37±22	31±17	0-82.7	0.1	13.5-20.2	17.8
West	30±6	214±55	39±10	32±8	0-5.8	0	16.6-19.7	18.5
East	21±5	151±39	21±10	19±7	0.6-72.6	3.2	11.8-19.2	14.9

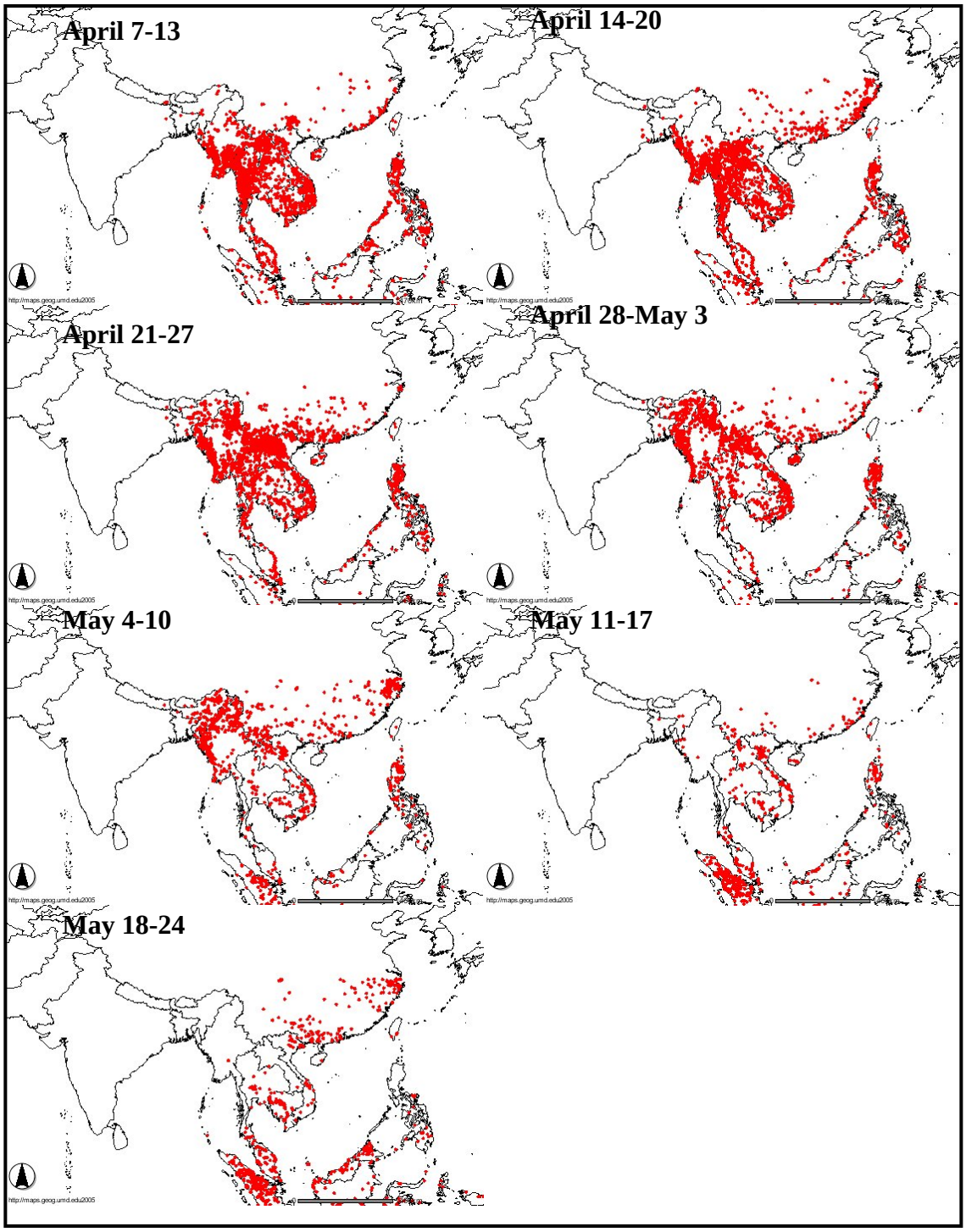

Figure 4.4. Geographical distribution of 7 d composite fire hot spots in Southeast Asia derived from MODIS data.

It is surprising to find that relatively lower concentration levels (O_3 = 21 ppb, CO = 151 ppb, $PM_{2.5}$ = 19 $\mu g/m^3$ PM_{10} = 21 $\mu g/m^3$) were associated with the eastern air masses. The air mass from this direction had to pass through many urban and industrial centres in Central and South China including the Pearl River Delta in Guangdong province. High levels of O_3 and O_3 precursors, such as VOCs and CO, were recorded in the air masses from these regions (Chan et al., 2002 and Wang et al., 2002). Pochanart et al. (2001) also reported low O_3 mixing ratios of 22–26 ppb for the northeastern Asian air mass. The authors believed that the dilution of continental O_3 by the inflow of fresh air from the Indian Ocean and the potential sink of O_3 during transport over the forest area of the tropics (Kirchhoff, 1998) is the reason behind this phenomenon. In our case, we noticed that there were much fewer fires in the eastern neighbour of Tengchong and in the SE and central China (Figure 4.4). This is the primary cause of the low pollutants observed in this air mass group. The air masses transported from the east were associated with rainy weather. The typical backward air trajectory together with the fire map are presented in Appendix I and II to show the effect of fire activities under the influences of eastern air masses. In fact, the rainfall record at our sampling site was 0.6–72.6 mm/d in this air mass group. It was raining everyday under this eastern air mass with a median rainfall of 3.2 mm/d, which was much higher than those of S/SW (0.1 mm/d) and western air masses (0 mm/d) (Table 4.2.). The mean temperature was also the lowest in this group (14.9^oC). The unstable atmosphere associated with rainy weather and lower temperature was not favorable for O_3 formation and pollution accumulation. As a result, a lower pollution level was observed even the air masses had passed over

polluted regions. We noted that the mean rainfall in eastern air mass was close to that of S/SW air mass. Yet, the concentrations of O_3, PM_{10} and $PM_{2.5}$ in S/SW air mass were much higher. This is due to the fact that there were more non-rainy days in the S/SW air mass group with elevated concentration episodes as results of transport of pollutants emitted from the active fire regimes in the south and west directions of Tengchong.

4.6. The effects of fire activities in the SE Asia subcontinent

The large variations of measured O_3, trace gases and aerosols were related to the fire activities in the SE Asia and the region close to the monitoring site. In this part of Asia, climate changes seasonally according to the monsoon flow. The wet season usually starts in May and ends in October whereas the dry season generally begins in November and ends in mid-April. The fire activities, as the result of burning agricultural residues, controlled by these seasonal weather changes, reach their full strength in the dry season in spring. Figure 4.4 presents the 7 d composite fire count maps for SE Asia derived from the MODIS data (http://maps.geog.umd.edu/maps.asp). In these maps, a hot spot represents a fire that lasted for at least 48 hr. In general, the fire hot spots decreased from April towards May and the hot spots decreased substantially after May. The majority of fires occurred in the SE Asia subcontinent. However, we noted there were suppressed fire activities in the Indo-Myanmar region of northern SE Asia subcontinent and its border to the eastern side of northern India Peninsula prior to 20 April. The fire activities in these regions resumed their strength afterwards until 10 May. The suppressed fire activities in the Indo-Myanmar region in the early period were due to the rainy weather (Figure 4.1). In this period, a maximum rainfall of 65.7 mm/d was recorded on 15 April. After that, fine weather prevailed until 10 May when the normal rainy season returned due to the on set of the southwest monsoon. Thus, the lower pollutant levels found at the beginning and end of the experimental periods were due to suppressed fire activities.

The higher pollutant levels in the middle of the experimental period were due to regional build-up of pollution as results of biomass-burning emissions associated with the fire activities. Figure 4.5 shows the time series of hourly averaged O_3, CO and aerosol concentrations from 20 April to 10 May when higher levels of O_3, trace gases and aerosols were observed. Two periods of elevated pollutant levels on 22–28 April and 5–10 May were observed. On 23–28 April, there were sharp increases of CO and $PM_{2.5}$ and PM_{10} until they reached the maximum at late night hours every day. The maximum hourly averaged concentrations of CO and $PM_{2.5}$ and PM_{10} reached 678 ppb, and 101 and 132 $\mu g/m^3$, respectively, on 24 April and 665 ppb, 7.7 ppb, 137 and 158 $\mu g/m^3$, respectively, on 26 April. High values were also observed on 23 and 25. The peak O_3 concentration occurred in the afternoon most of the time. In the second episode, O_3 precursor, CO, together with aerosols had sharp increases from 18:00 on 5 May. They attained their peak levels at about the late night of 5 May and the early morning of 6 May and sustained their high concentrations until around the early afternoon of 6 May forming a broad high pollutant regime. This phenomenon was unusual when compared with their averaged diurnal variation plotted in Figure 4.2. The maximum concentrations of CO and $PM_{2.5}$ and PM_{10} reached 433 ppb, and 125 and 144 $\mu g/m^3$, respectively. An O_3 hourly maximum of 59 ppb occurred at 10:00 on 6 May. The high O_3 levels sustained until afternoon. The usual O_3 peak occurred at 14:00.

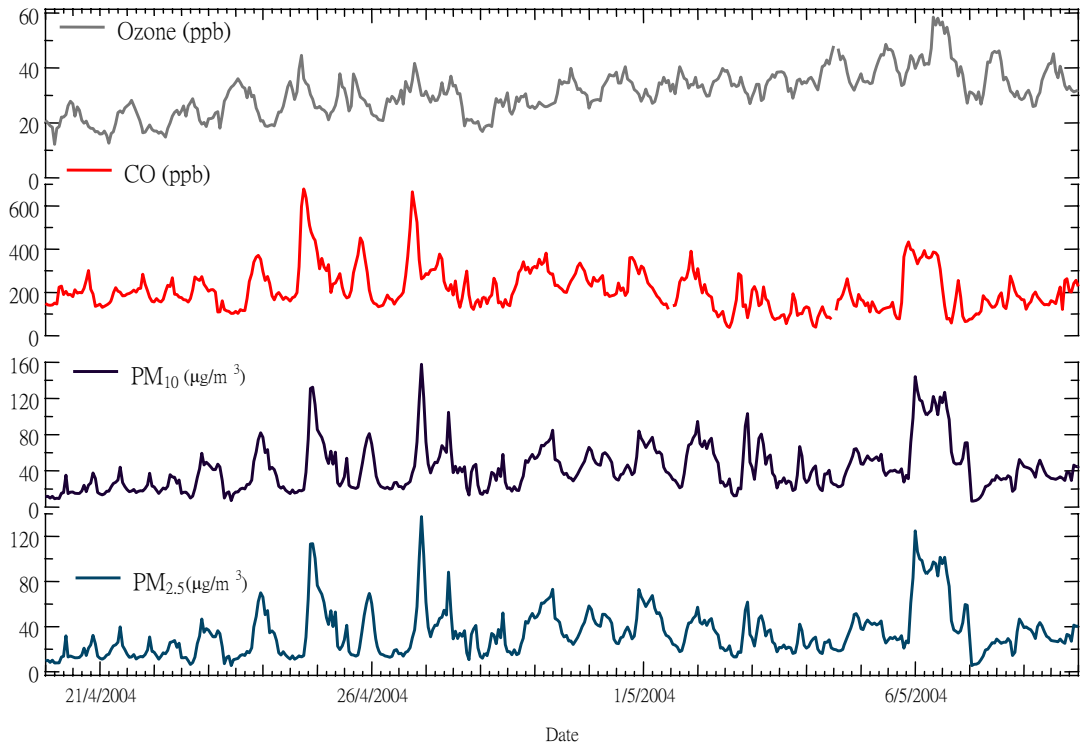

Figure 4.5. Hourly concentrations of O_3, CO, PM_{10} and $PM_{2.5}$ from 20 April to 10 May

Figure 4.6. shows the 5 d backward air trajectories at the surface layer (600, 800 and 1000 m) on 25 and 27 April, and 5 May when high pollution levels were found. The air masses at the surface originated from the close vicinity of the Bay of Bengal and passed over Bangladesh, Bhutan and Myanmar region in the close neighbourhoods of Tengchong, where active fires were found (Figure 4.4). There were upward motions when the air masses passed over these active fire regions. Liu et al (1999), Chan et al. (2000) and Chan et al. (2003c) found that the air masses having passed over these regions had high O_3 as observed over SE China in Hong Kong. The back air trajectory and fire map suggested that it was the result of regional photochemical O_3 formation and accumulation involving the high levels of

O_3 precursors during the trans-boundary transport to Southwest China under favorable meteorological conditions.

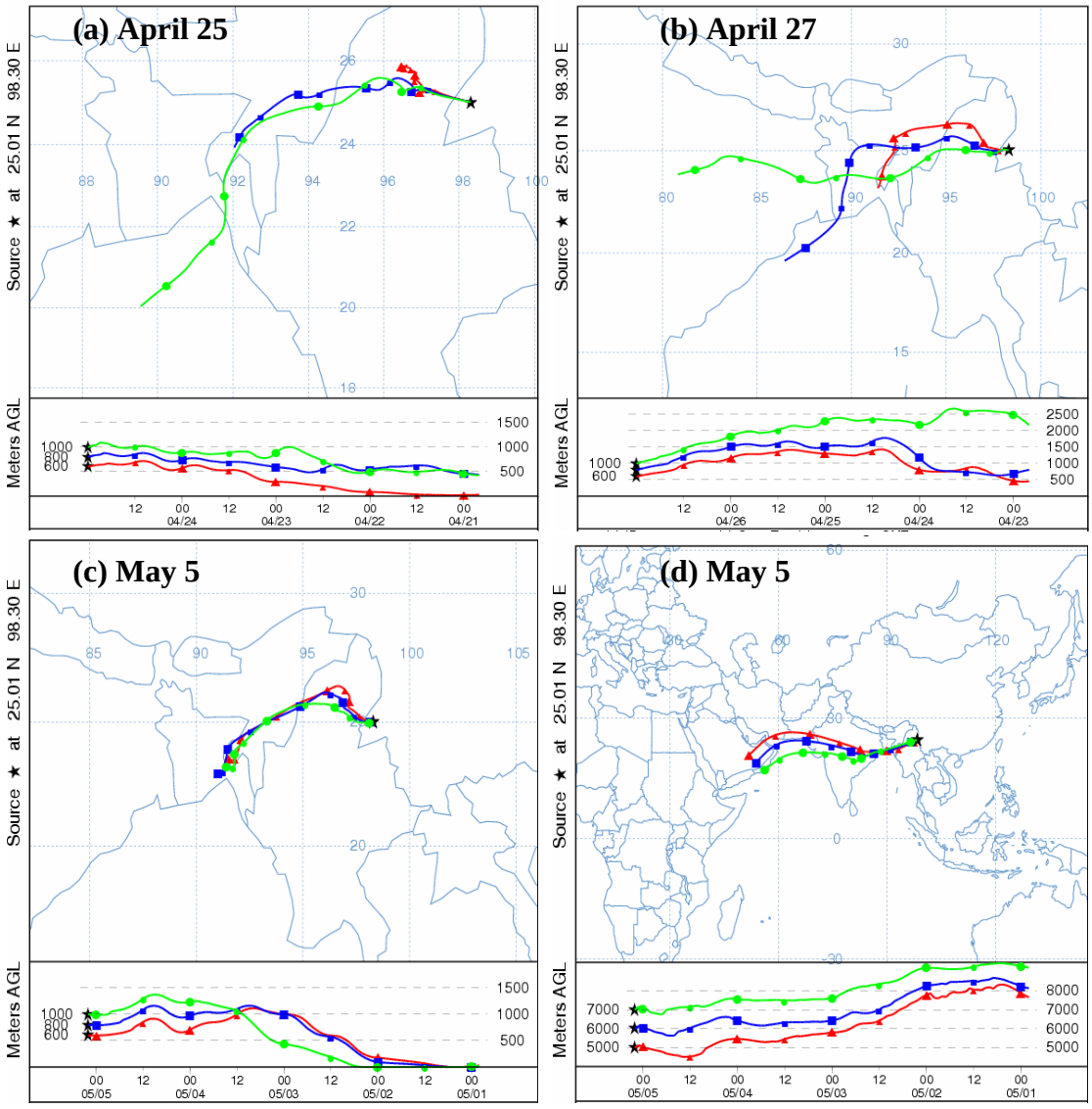

Figure 4.6. Five-day backward air trajectories reaching Tengchong at 600, 800 and 1000 m on (a) April 25, (b) 27 and (c) May 5 and (d) 5000, 6000 and 7000 m on May 5.

4.7. Biomass burning tracers in aerosol on ozone episode

Water-soluble potassium (K^+) is a typical component of biomass burning aerosol. To clearly identify the source of air masses in our episode cases, K^+ has been used as tracer element for the qualitative identification of biomass burning (Cachier et al., 1991; Chow, 1995). Before applying the water-soluble K^+ as a tracer of biomass burning, the contribution of nss-K^+ should be distinguished. By the equation [2.1], all the samples of particulate K^+ contain at least 68% of nns-K^+ (Figure 4.7). This fact suggested that the sources of K^+ were mainly from the biomass burning emission, and were not from the sea salt particulate.

The average concentration of water soluble K^+ in PM_{10} was 0.23 μg/m^3, ranging from 0.04 - 0.55 ug/m^3 in our sampling period. Duan et al. (2004) reported that the annual average concentration of K^+ in Total Suspended Particulate (TSP) at the rural site of Beijing, China, was 1.21ug/m^3. Ho et al. (2003) found that the concentrations of K^+ in PM_{10} and $PM_{2.5}$ were 0.72 and 0.68 μg/m^3 respectively at the background site of Hong Kong, China. The concentration level of water soluble K^+ in Tibetan Plateau was relatively lower comparing with other developed cities in China.

As discussed in the previous section, two elevated pollutant levels on 22-28 April and 5-10 May were observed. Results indicated that the air masses were origin from the active fire regions by the meteorological approaches. In these two periods, enhanced water soluble K^+ ions were also detected. The concentrations of water soluble K^+ were 0.55 ug/m^3 on 24-25 April and 0.48 ug/m^3 on 5-6 May, which were 139% and 109% higher than the average concentration levels, respectively (Figure

4.8). This fact strongly suggested that the ozone and its precursors were origin from the biomass burnings by the chemical approaches.

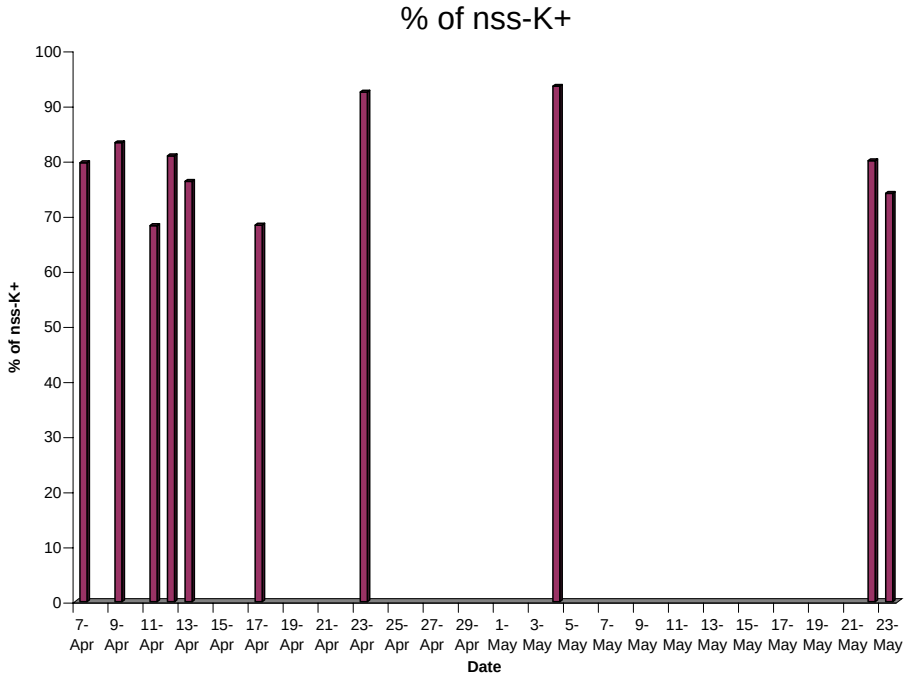

Figure 4.7. Percentage of nss-K+ during the sampling period

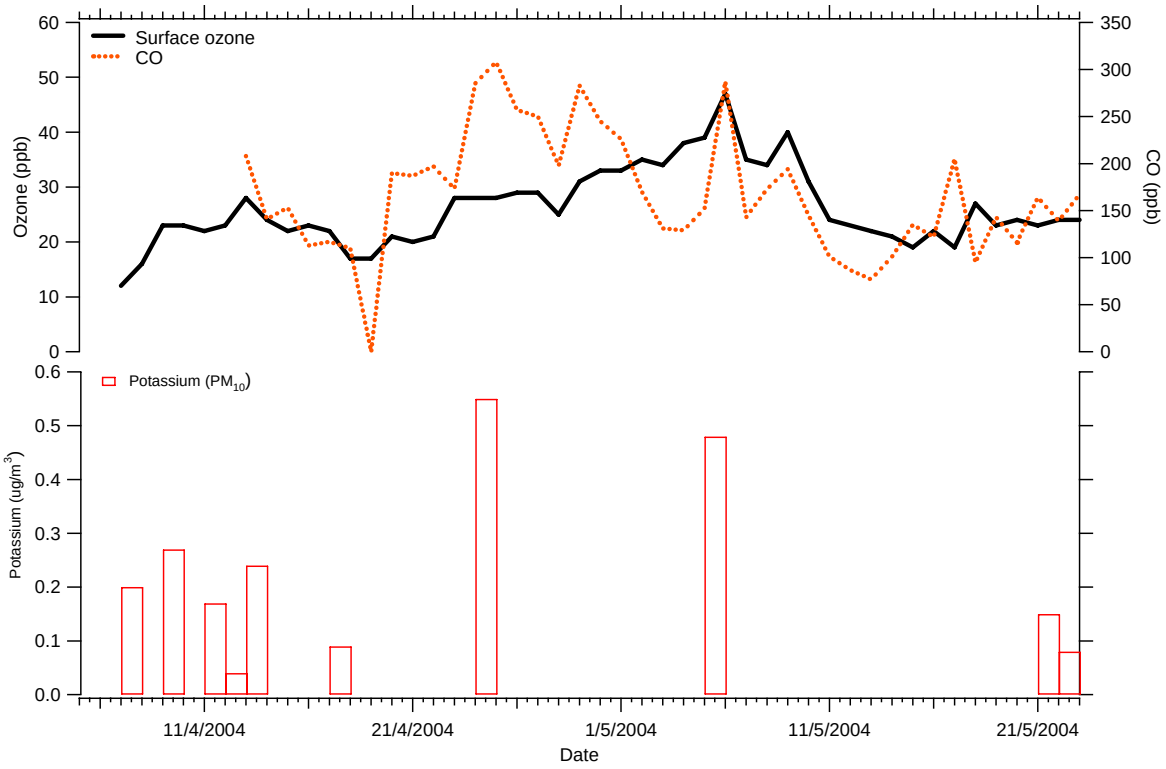

Figure 4.8. Daily average concentrations of O_3, CO and water soluble potassium ion during the sampling period.

4.8. Conclusion

There are limited measurements of tropospheric O_3, trace gases and aerosols in the background atmosphere of tropical and subtropical Asia and China despite the rapid urban, industrial and agricultural development in the region in the last two decades. Our surface O_3, CO and $PM_{2.5}$ and PM_{10} measurements as well as the water-soluble K^+ ions in the spring of 2004 over the Tibetan Plateau in Tengchong showed that the pollutant levels in this relatively undeveloped region of Southwest China were impacted by the biomass-burning emissions associated with fire activities in the SE Asian subcontinent and pollution transport from South Asia based on the meteorological and chemical approaches. A comparison of the O_3 concentration measured in Tengchong with those in similar longitudinal sites in SE Asia and northeastern Tibetan Plateau suggested that there existed complex variations of O_3 in the Tibetan Plateau and its neighboring SE Asian region. Back air trajectory analysis revealed that the air masses from the west and south direction that had passed through the Myanmar–Bangladesh region of SE Asia and northeastern India Peninsula of South Asia had the higher O_3, CO and aerosols when compared with the air mass associated with the Northeast Asian monsoon, which had passed over large urban and industrial centers of Central and South China. The findings indicated that the regional built-up of air pollution and transport of the biomass-burning emissions and pollutants from these regions was an important source of trace gases and aerosols in this relatively undeveloped region of western China. The emissions in SE Asia and South Asia had relatively stronger impacts than the urban and industrial emissions in the Central and South China on the abundance of trace

gases and aerosol in the background atmosphere over the Tibetan Plateau of Southwest China based on the measurement data in the spring of 2004.

CHAPTER 5 - EFFECTS OF KOREAN FOREST FIRES ON THE ATMOSPHERE OF NORTHEASTERN CHINA IN THE SPRING OF 2005

5.1. Introduction

Arbor Day is a festival in Asian countries at which people traditionally clean and weed the areas around their ancestors' tombs and perform ancestral memorial rites. Consequently, chances for accidental fires are very high around this time of the year. Forest fires on Arbor Day in Korea during the last 5 years from 2000 led to 1167 hectares of woodland being burned, which is 3.4 times the area of Nam Mountain in Seoul (KBS World Radio). But this time, the 2005 Korean forest fires, which started from routine burning for land clearing, soon got out of control and spread over a wide area. The fire erupted around 11:50 p.m. on 4 April, 2005 near the border between North and South Korea and came under control by 6 April, destroying more than 400 hectares of woodland. Twenty one mountainous areas nationwide were engulfed (Figure 5.1). The government declared disaster emergency and thousands of people in Yangyang and Kangwon Provinces, Korea were evacuated on 5 April (The Korea Times).

In this study, a case study was presented attributing the 2005 Korean forest fires as the sources of O_3, CO, hydrocarbons and particulate enhancement in the lower troposphere and within the boundary layer at the northeastern Heilongjiang Province, China in spring of 2005. Ground-based measurements of O_3 and CO as well as non-methane hydrocarbons (NMHCs), fire counts from Along Track, Scanning Radiometer (ATSR) satellite imagery from the European Space Agency

(ESA), TOMS absorbing aerosol index (AI) product from NASA and global gridded final run (FNL) meteorological data from NOAA were used to assess the extent of impact in northeastern China

Figure 5.1. A fireman struggles with a forest fire fanned by strong winds in Yangyang, Kangwon Provenice, on Arbor Day (The Korean Times)

5.2. Comparison of ground-based continuous measurements with other monitoring sites

The springtime average concentrations of O_3 and CO during the whole sampling period were 43 and 243 ppb respectively. The springtime surface O_3 and CO in Northeastern China were higher when compared with another background site situated on relatively undeveloped region in China at the same period of the year. In Chapter 4, the concentrations of trace gases and aerosols were measured. The surface O_3 and CO over the Tibetan Plateau at Tengchong were 26 and 179 ppb respectively (Chan et al., 2006). The lower pollution levels in subtropical Southwestern China are due to the lesser anthropogenic impact in this undeveloped region, and humid tropical climate resulting from the inflow of marine air mass from the Indian Ocean and the South China Sea in spring. In contrast, Heilongjiang province is located in the extreme northeastern part of China. The climate is entirely dominated by the alternating continental and maritime monsoons. Frost and snow play a major role from September to May with drier atmosphere whereas July is the wet month with a marked summer peak of precipitation, normally accounting for 50-60% of the annual precipitation (600-800 mm). It is still under the influence of the Siberian continental high-pressure system in spring, resulting in drier atmosphere and lower precipitation, which are more favorable for pollution accumulation. However, the concentration levels were lower than or similar to those reported for other rural sites in China and East Asia. Wang et al. (2001) found that the concentrations of O_3 and CO were about 50 ppb and 600 ppb respectively on the East China coast within the Yangzhi River Delta in Linan. Chan et al. (2002)

reported surface O_3 and CO values of 30 ppb and 300 ppb, respectively for the subtropical South China coast within the Pearl River Delta in Hong Kong. Pochanart et al. (1999) stated that the mean concentrations of O_3 and CO were about 49 ppb and 236 ppb, respectively at the Oki Island in East Asian Japan.

5.3. Diurnal cycle and daily variation of surface O_3 and CO

The averaged diurnal variations of surface O_3 and CO during the sampling period were plotted in Figure 5.2. The ozone profile exhibited a minimum of ~37 ppb at 6:00 in the morning, gradually increased to a peak of ~ 50 ppb in the late afternoon at 15:00, and then followed by a gradual decrease until the following morning. Conversely, CO showed a trough in the afternoon and an increasing trend was observed from 16:00 until it reached the peak with ~260 ppb in the evening at 19:00. The diurnal cycles of CO and O_3 at Long Fengshan station in spring were similar to those at other rural areas in China such as Linan in eastern China (Wong et al., 2001) and my previous study (Chapter 4) at Tengchong in southwestern China (Chan et al., 2006).

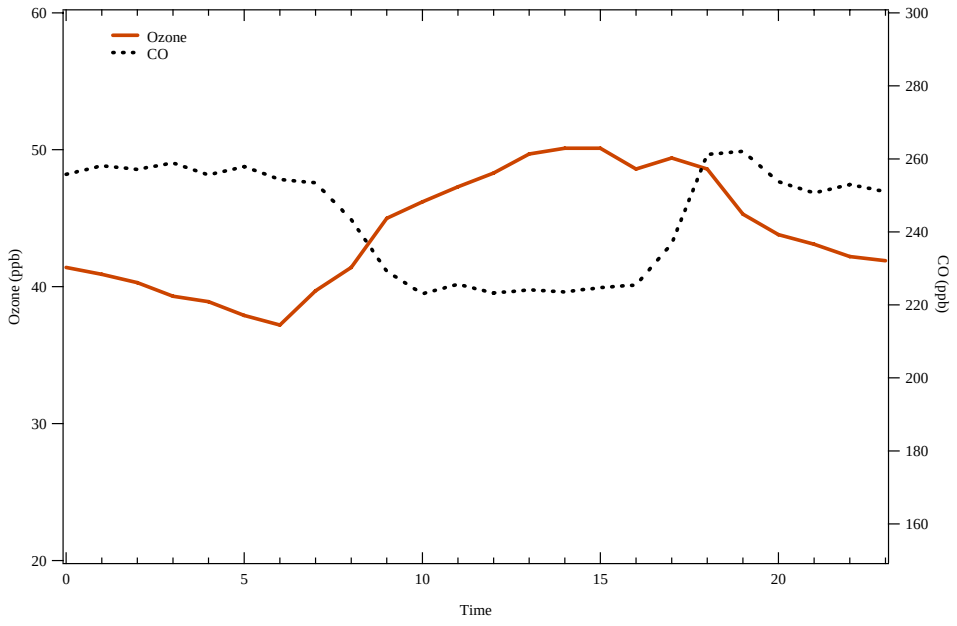

Figure 5.2. Diurnal variations of O_3 and CO in the spring of 2005

5.4. Ozone episode observed at Long Fengshan station

The daily variation of concentrations of CO and O_3 as well as the rainfall was plotted on Figure 5.3. Surprisingly, high concentration levels were observed on 5 April in this background station with daily average concentrations of 78 ppb for O_3 and 618 ppb for CO, which are about 80 and 150% higher than the average concentrations. We thus extracted this part and depicted it in Figure 5.4. In this episode, the O_3 precursor, CO, built up at the night time on 4 April and reached the daily maximum of 765 ppb at 1:00 on 5 April, and maximum ozone concentration of 97 ppb was observed at 15:00 on 5 April. We also noticed that the peaks for O_3 and CO were simultaneously reached at 4:00 on 6 April, which was unusual when compared with their average diurnal variation plotted in Figure 5.2.

Because CO is one of the O_3 precursors and was found to be a useful indicator of anthropogenic pollutants with a long enough lifetime, correlation between CO and O_3 could be used to demonstrate photochemical activities at a regional scale. Simple linear regression correlations between hourly averaged concentration levels of O_3 and CO were calculated for the entire sampling data (41 days, 940 hr). Significant testing for correlation analysis was done. As the P value of the linear regression equals to zero, the coefficient have significant difference to zero. For the entire data set, the average slope (O_3/CO) and correlation coefficients (R) were 0.071 and 0.54 respectively. It is comparable with those at another East Asian remote site in Oki, Japan (Pochanart et al., 1999) during the springtime period. The weak correlation between O_3 and CO in springtime might reflect the fact that the photochemical activity was lower in spring. Heilongjiang is located between the

temperate and the frigid zones with continental monsoon climate. The average temperature in spring was about 5^{o}C with longer night time but shorter daytime. It is unfavorable for O_3 production and the photochemical reaction is still suppressed to a lower rate. In this episode on 4-6 April, better correlation of O_3 and CO (R=0.66) was obtained. This feature reflects the influence of the intense Korean fire activity impact. In the next section, this episode is further analyzed with the help of fire count from MODIS data, TOMS Aerosol Index data from NASA and synoptic weather pattern from NOAA.

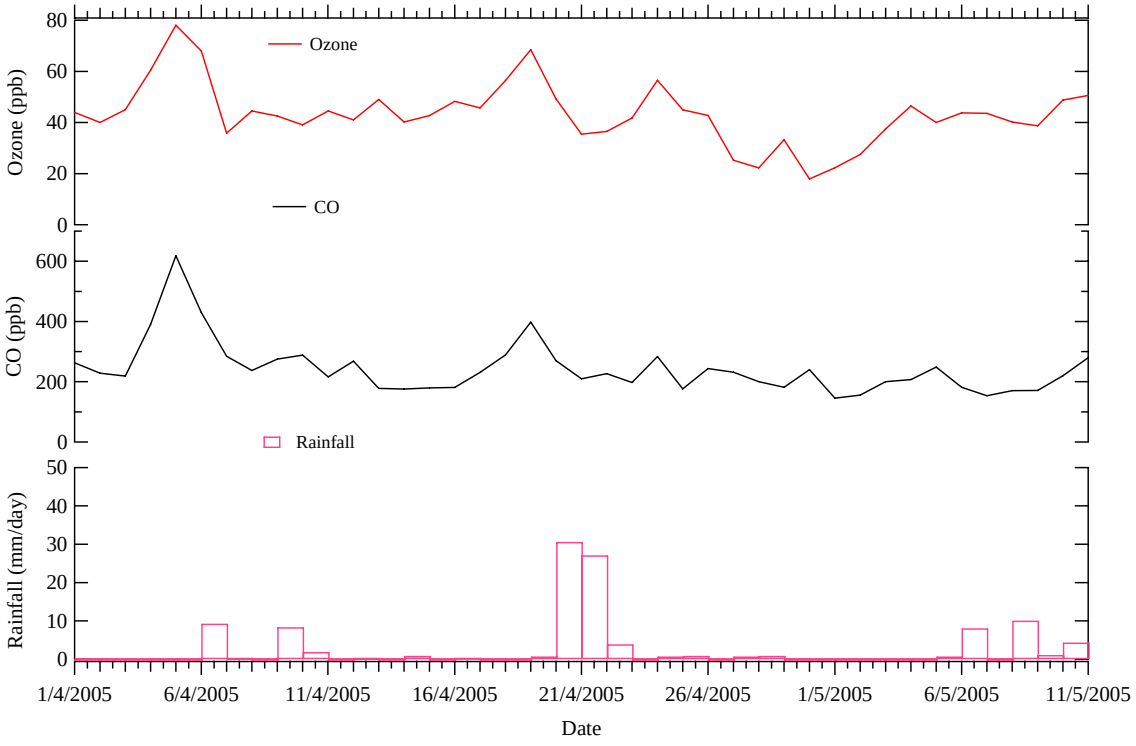

Figure 5.3. Daily variations of O_3, CO and rainfall during the spring of 2005.

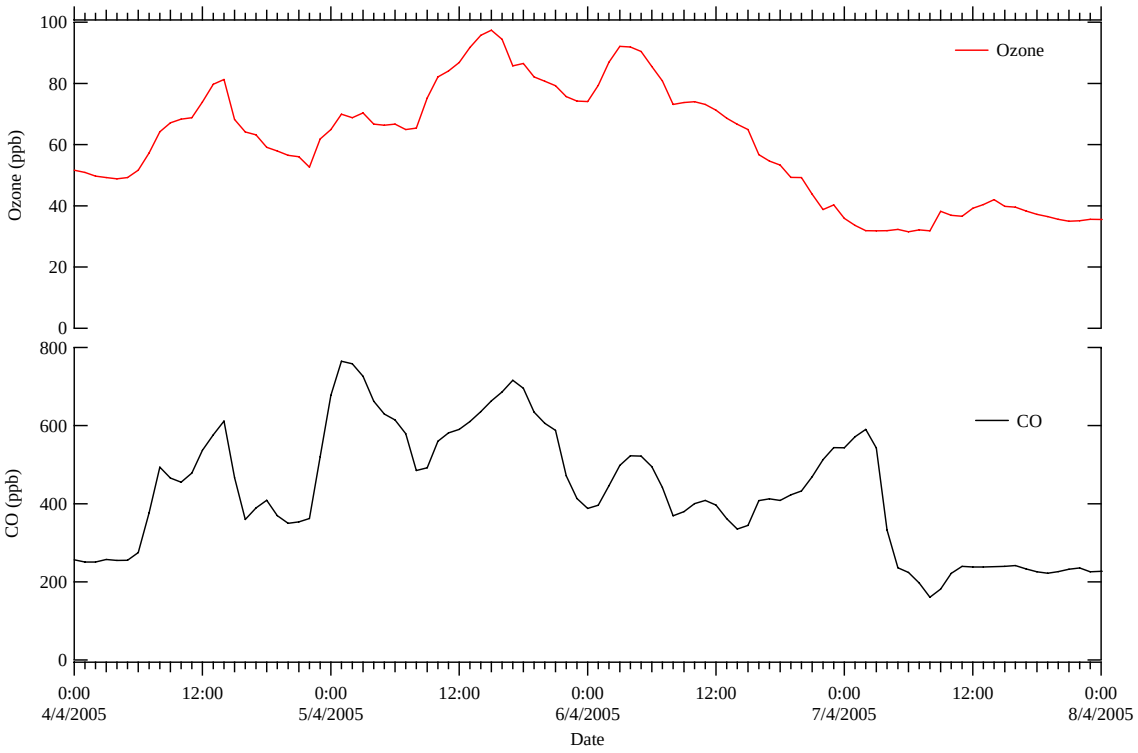

Figure 5.4. Hourly concentrations of O_3 and CO from 4 to 8 April

5.5. Evidences of horizontal transport from Korean forest fires

5.5.1. Hot spots detected by satellite image

Recent studies revealed that the boreal forest fires in high northern latitudes produce large amounts of smoke, CO and O_3 with considerable horizontal and vertical transport (Kato et al., 2002; Tanimoto et al., 2000; Fromm et al., 2000; Westphal and Toon, 1991; Chung, 1986). It was noteworthy in the case of horizontal transport of pollutants in our study. Fire map was used to confirm the severity of Korean forest fire. Figure 5 shows the active fire at East Asia on 5 April, marked with red dots, which were produced from the ATSR world fire atlas. Significant hot spots were observed at the border of North and South Korea on 5 April, 2005, which was consistent with the period and location of the Korean forest fires reported. These fire activities resulted in the emission of O_3 precursors such as CO, methane, non-methane hydrocarbons and smoke aerosol into the atmosphere of nearby regions.

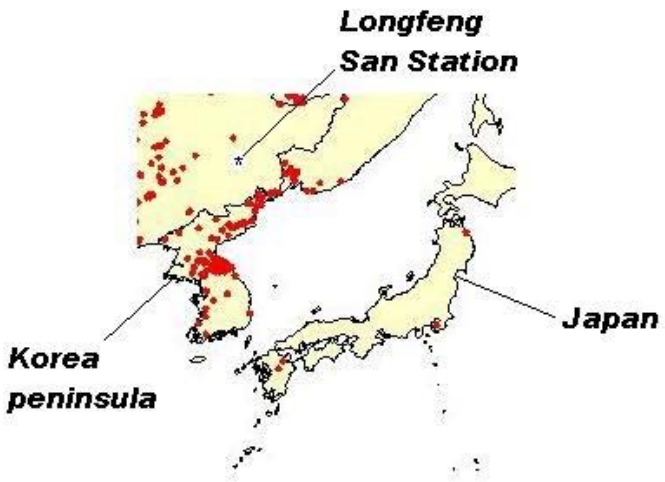

Figure 5.5. Fire hot spots in East Asia derived from MODIS data.

5.5.2. Synoptic analysis by meteorological data

Generally, the transport of pollutants from emissions depends on the direction of airflow. In North Asia, a continental high-pressure system normally lies in the middle of the Eurasian continent except during summer. Thus, the prevailing airflows in the Pacific Rim region are generally northeasterly or westerly with outflow to Japan and the West Pacific depending on the location of the continental high-pressure system (Kajii et al., 1997, Pochanart et al., 1999). Kajii et al. (2002) showed that the fires burned in south central Siberia and Mongolia in the vicinity of Lake Baikal were usually observed in the Happo research station, Japan, under the general airflow patterns in continental rim region (Figure 5.6.).

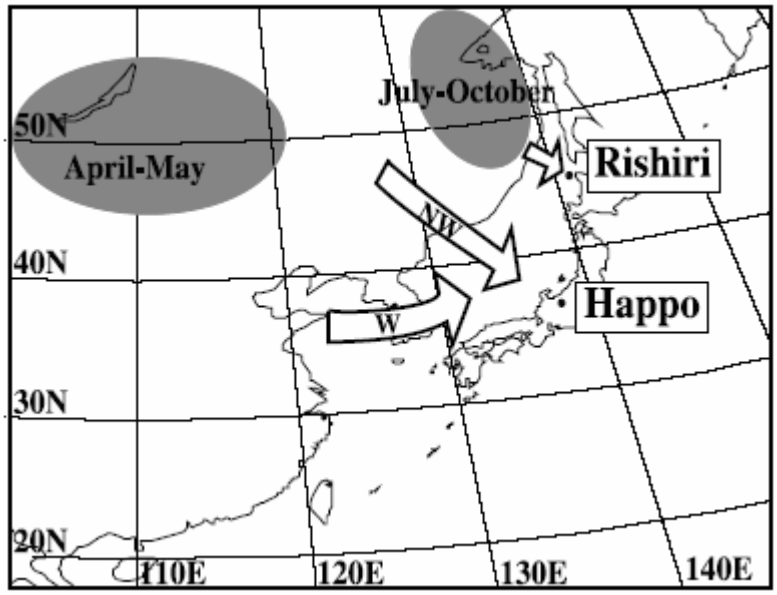

Figure 5.6. General airflow patterns in continental rim region in North Asia (Kajii, et al., 2002)

However, the transport pathway of pollution in our case is different from previous studies. The pressure chart and wind vector (Figure 5.7 & 5.8) at the surface level during 4-6 April were used to indicate the airflows in our study region. Firstly, a low pressure system was observed at eastern Russia, near the Chinese border on 4 April. It moved southwesterly to eastern Inner Mongolia on 5 April and then moved to Heilongjiang Province on 6 April. This low pressure with mean sea-level pressure of 991.15 hpa changed the surface wind to move northward from East China Sea and Yellow Sea, crossing the Korean Peninsula and finally reached our sampling site.

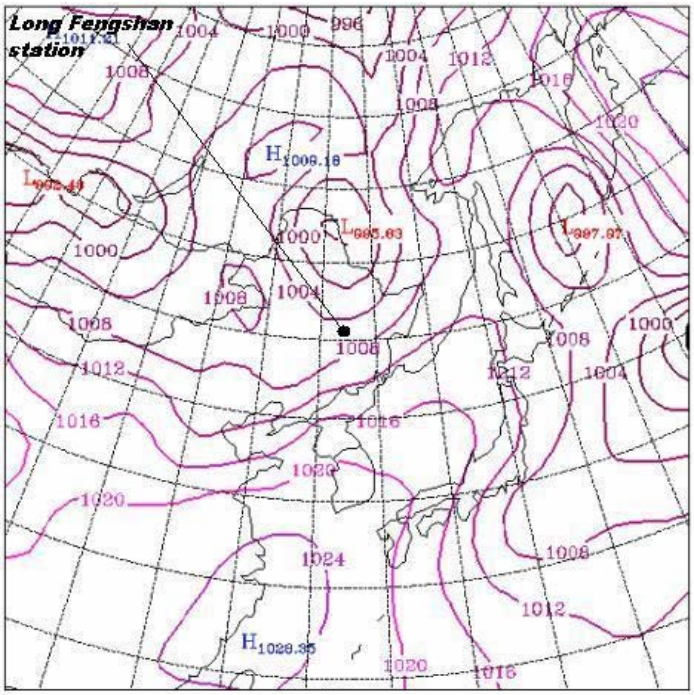

Figure 5.7a. 04 April 2005

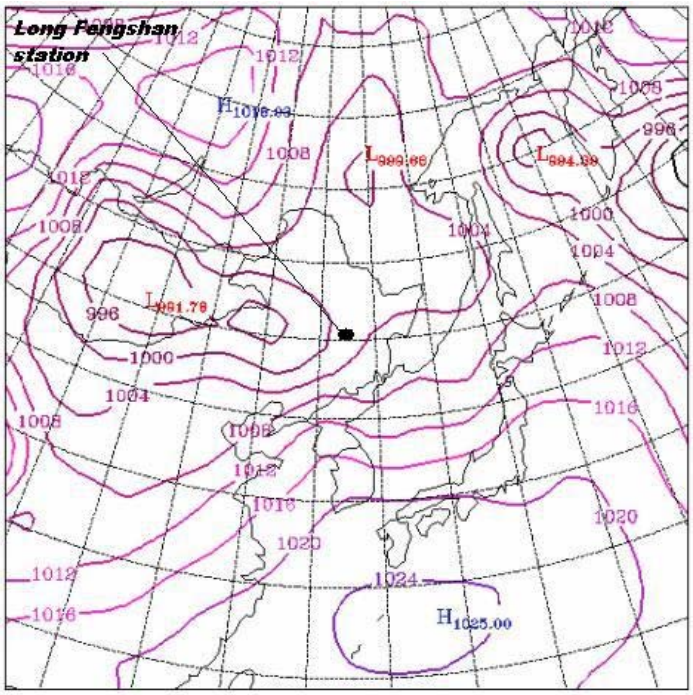

Figure 5.7b. 05 April 2005

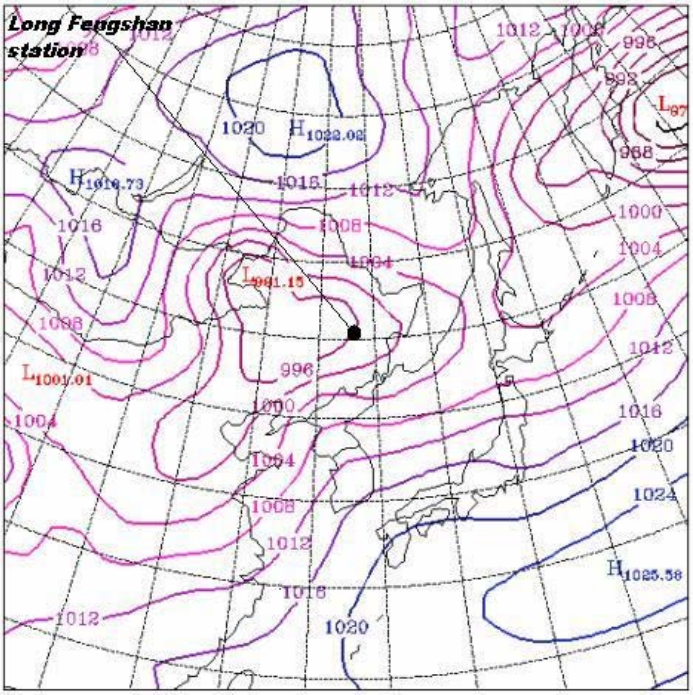

Figure 5.7c. 06 April 2005

Figure 5.7. Pressure chart in northeastern China from 4-6 April 2005.

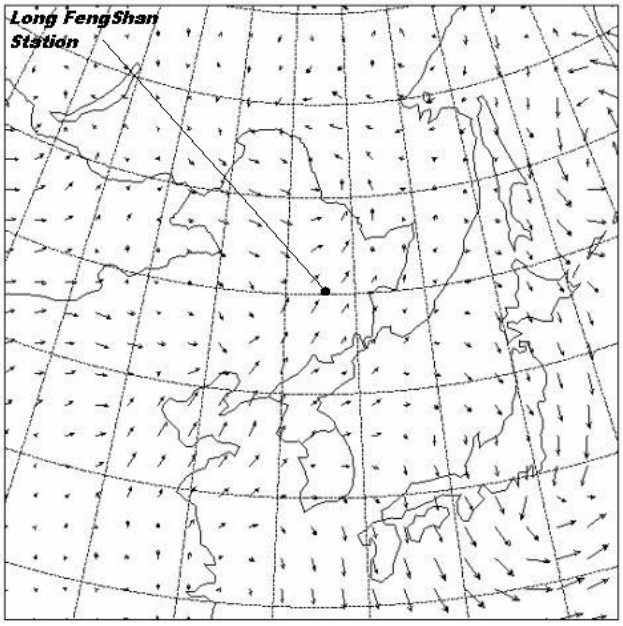

Figure 5.8a. 04 April 2005

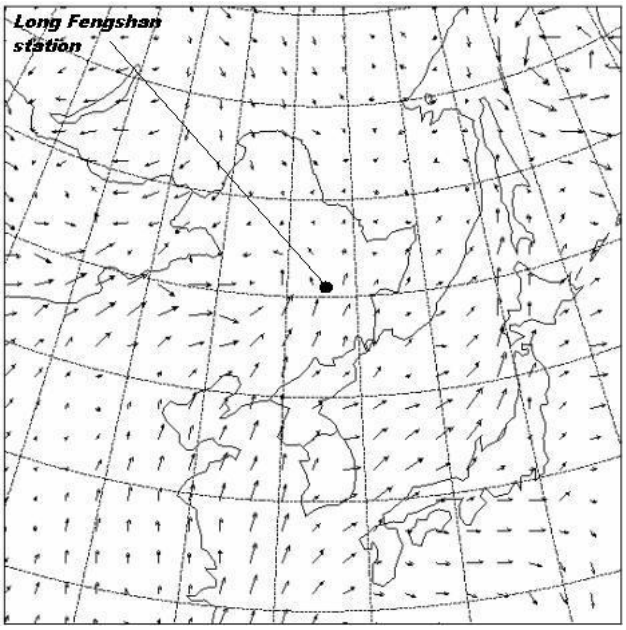

Figure 5.8b.05 April 2005

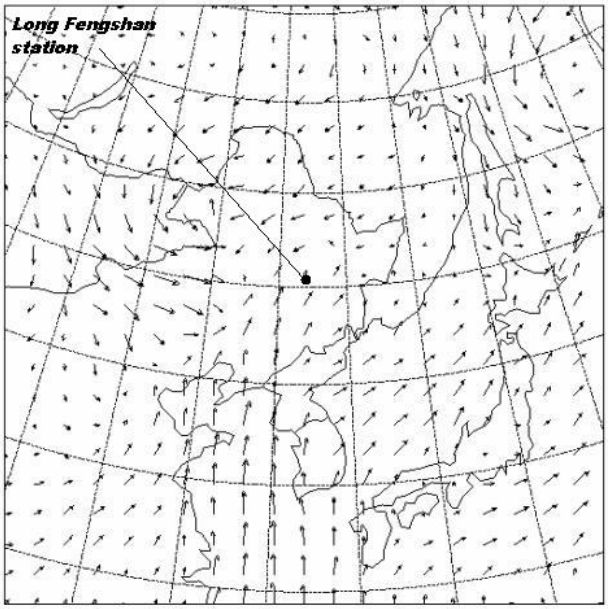

Figure 5.8c. 06 April 2005

Figure 5.8. Surface wind vector from 4-6 April 2005

5.5.3. Smoky plume detected by TOMS data

TOMS AI data was analyzed in order to investigate the impact of the Korean Forest fire emissions on northeastern China. Figure 5.9. shows the TOMS Aerosol Index (AI) over northeast Asia. Generally, positive AI values reflect the presence of absorbing aerosols and negative AI for non-absorbing aerosols. We observed the smoke plume emitted from the Korean peninsula on 4 April. It moved northward toward northeastern China on 5 April following the direction of surface wind described above. Eventually, an extremely heavy smoke plume with AI index ~ 3.5 obscured the land and spread over vast area of northeastern China on 6 April. The plume index became more dispersed and obscured three northeastern Chinese

Provinces of Heilongjiang, Jilin and Liaoning with a total land area of about 790,000 km^2, which is more than three times the total land area of England (240,000 km^2).

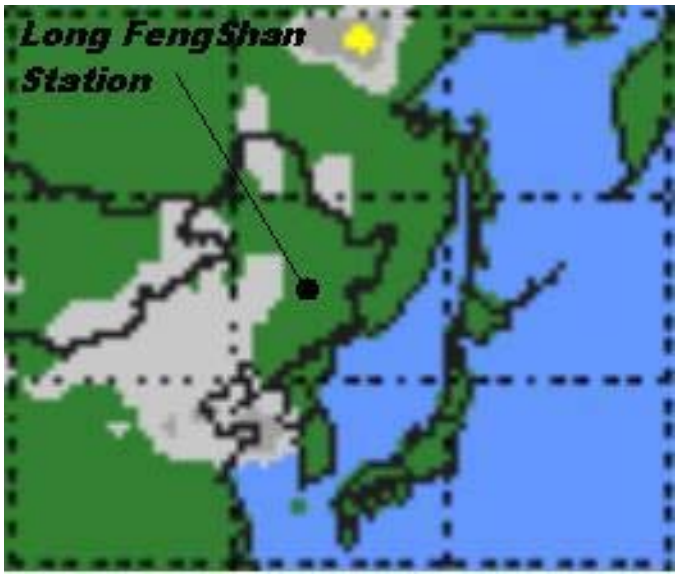

Figure 5.9a. 04 April 2005

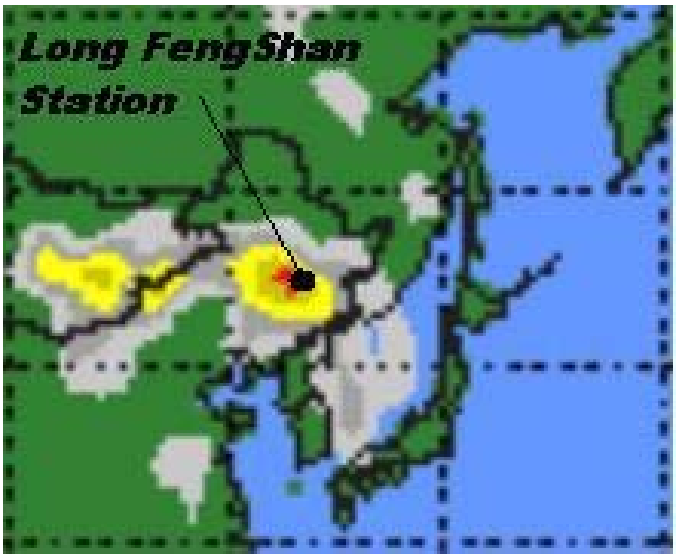

Figure 5.9b. 05 April 2005

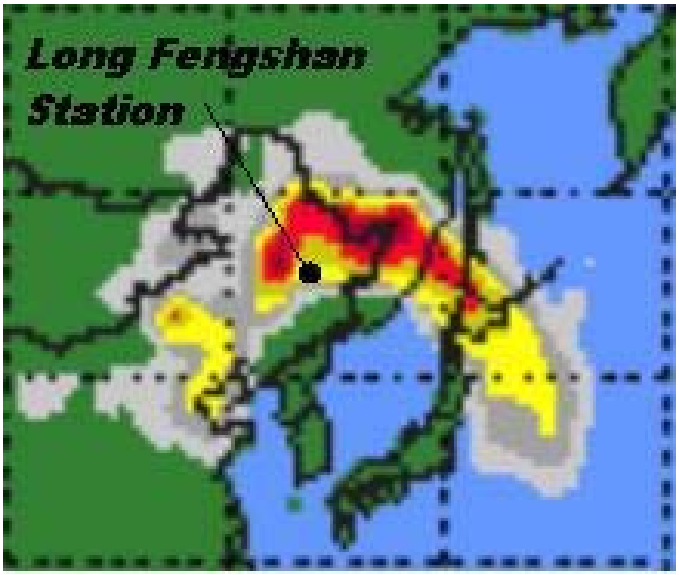

Figure 5.9c. 06 April 2005

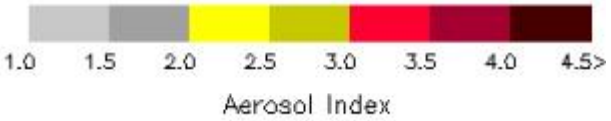

Figure 5.9. TOMS aerosol index map for the period 4-6 April 2005.

5.5.4 Compare the pollution levels with and without the effect of Korean Forest Fire

In order to exanimate the pollution levels without the effect of Korean forest fires, similar wind direction period but without Korean forest fires was found, during the sampling periods. It serves as a comparison between the observed data with and without the effect of Korean forest fires for evaluating the magnitude of the influence of Korean forest fire on the atmosphere of Northeast China.

The average concentrations of O_3 and CO were 43 and 243 ppb respectively. During the period of Korean forest fire, the daily concentrations of O_3 and CO were 78 and 618 ppb. On 19 April without the effect of Korean forest fire, the daily

concentrations of O_3 and CO were 68 and 397 ppb. Therefore, the Korean forest fire could enhance the pollution levels in our sampling site.

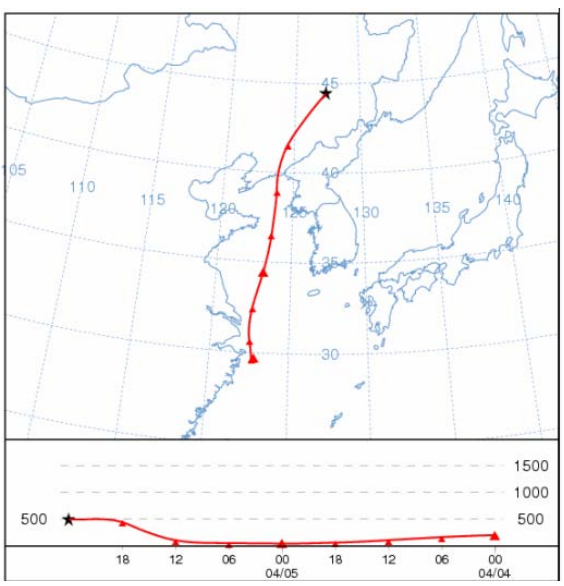

Figure 5.10a) 06 April 2005

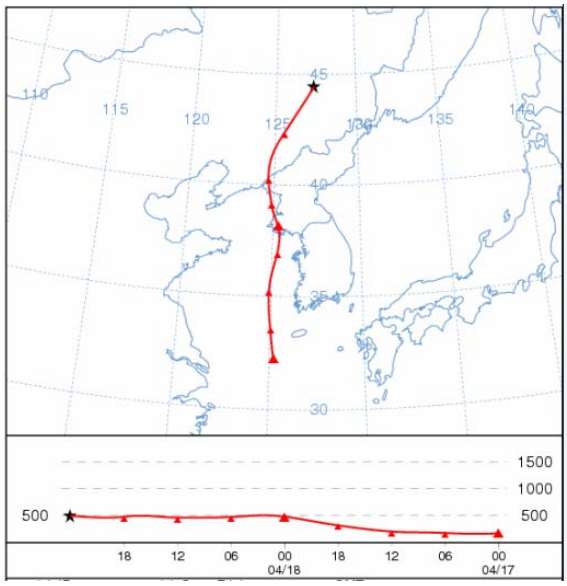

Figure 5.10b) 19 April 2005

Figure 5.10.) Backward air trajectory in Long Fengshan WMO Regional Background Station on 06 and 19 April 2005

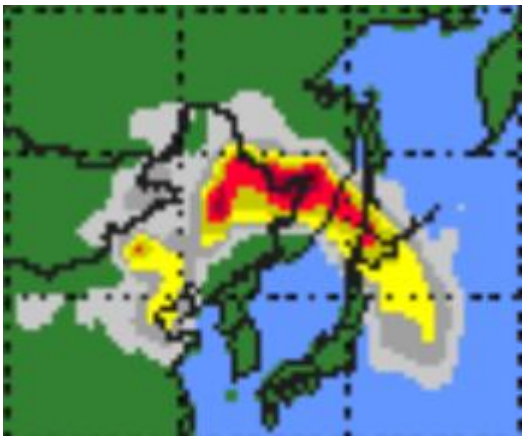

Figure 5.11a) 06 April 2005

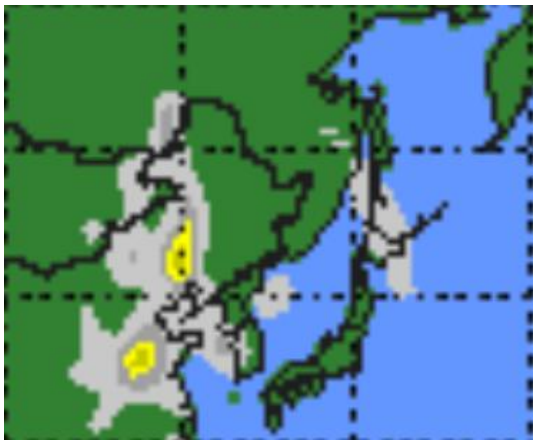

Figure 5.11b) 19 April 2005

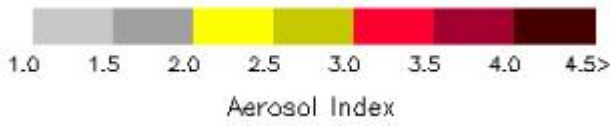

Figure 5.11) TOMS AI map in northeastern China on 06 and 19 April 2005

5.6. Biomass burning tracers in VOCs during the Korean forest fires period

The concentration ratio of ethane to propane is wildly used to investigate the emission characteristics of various source regions and relative age of the air mass (Talbot et al., 1997; Carmichael et al. 2003; Russo et al., 2003; Wang et al. 2003, 2005). Fossil fuel combustion, biomass burning, natural gas and liquefied petroleum gas (LPG) are the major sources of ethane, while natural gas, LPG and biomass burning are the major sources of propane (Choi et al., 2003). The ethane/propane ratio can reflect the differences in contribution of biomass burning, biofuel combustion and transportation. High value indicates regions with tropical forests fire and large biomass burnings. Intermediate value reflects a blend of biofuel and biomass usage, and the small value reflects industrial regions dominated by fossil fuel usage (Carmichael et al. 2003). Carmichael et al. (2003) reported that the distribution of ethane/propane ratios was 1.5 – 2.5 in northeastern China and 1 – 6 in Asia. In my study, the ethane/propane ratio is 2.4 during the springtime, which is within the range of the previous study. However, a high ethane/propane ratio of 3.1 was observed in our station during the period of Korean forest fire implicating that northeastern China was under the influence of the Korean forest fire activities.

Emissions from open burning are greater than those from well-controlled combustion sources (Lemieux et al., 2004). Studies had shown that large amount of volatile organic compounds (VOCs), such as butadiene (70 mg/kg burned), benzene (230 mg/kg burned), toluene (130 mg/kg burned), xylenes (45 mg/kg burned), ethylbenzene (13 mg/kg burned), styrene (24 mg/kg burned) and others could be emitted into the atmosphere from the burnings of biomass. In my study, the average

concentrations of the aromatics hydrocarbons of benzene (B), toluene (T), ethylbenzene (E) and xylenes (X) were 0.334, 0.123, 0.031 and 0.022 ppbv, respectively. During the period of Korean forest fire on 4 April, high concentrations of aromatics hydrocarbons were observed. The concentrations of BTEX were 0.725, 0.343, 0.083 and 0.624 ppbv respectively, which are much higher than the average concentration levels. VOCs are known to be ozone precursors (Carter, 1994). Base on the concept of maximum increment reactivity (MIR) of ozone formation, emissions from the biomass burnings could have high potential to cause ozone formation. An induced high ozone concentration of 97 ppb was thus observed at 16:00 on 5 April (Figure 5.4.), during the period of Korean forest fires.

5.7. Conclusion

In this Chapter, surface O_3 and CO as well as NMHCs were measured at the remote site of northeastern Heilongjiang Province in the spring of 2005. At the beginning of April, Intensive Korean forest fires induced at the Arbor Day by the ancestral memorial rites occurred at the Koran Peninsula. Large amount of O_3 precursors and aerosol were suddenly released to the atmosphere in a matter of hours. The impacts of the Korean forest fires were investigated with the help of satellite data and the ground-based measurement setup in our station. Abnormal high concentrations of surface O_3 and CO as well as the ozone precursors (VOCs) were observed within the period of the Korean forest fires. It was the first recording of adverse air pollution effect resulted from Korean forest fires over northeastern China. Additionally, observations from the TOMS AI suggested that the smoky plume from the forest fire emissions could disperse and obscure a vast land area of the northeastern part of China under normal meteorological conditions.

CHAPTER 6 – CONCLUSION

In this study, two comprehensive field measurements were performed at the remote sites of China in the springs of 2004 and 2005, where observation data is scare. In the first phase of study in the spring of 2004, surface O_3 and its precursor CO and aerosols over the Tibetan Plateau were measured at the southwestern border of China, whereas in the spring of 2005, O_3 and CO as well as NMHCs were measured at the Long Fengshan World Meteorological Organization (WMO) Regional Background Station at Northeastern Heilongjiang Province. During spring, biomass burnings and forest fires are active in Asia. The effects of emissions from Asian open burnings to the remote sites of China were analyzed in this study with the help of satellite data.

Our surface O_3, CO and $PM_{2.5}$ and PM_{10} measurements as well as the water-soluble K^+ ions in the spring of 2004 over the Tibetan Plateau in Tengchong showed that the pollutant levels in this relatively undeveloped region of Southwest China were impacted by the biomass-burning emissions associated with fire activities in the SE Asian subcontinent and pollution transport from South Asia based on the physical and chemical approaches. A comparison of the O_3 concentration measured in Tengchong with those in similar longitudinal sites in SE Asia and northeastern Tibetan Plateau suggested that there existed complex variations of O_3 in the Tibetan Plateau and its neighboring SE Asian region. The findings indicated that the regional built-up of air pollution and transport of the biomass-burning emissions and pollutants from these regions was an important source of trace gases and aerosols in this relatively undeveloped region of western China. The emissions in SE Asia and South Asia had relatively stronger impacts than the urban and

industrial emissions in the Central and South China on the abundance of trace gases and aerosol in the background atmosphere over the Tibetan Plateau of Southwest China based on the measurement data in the spring of 2004.

Intense Korean forest fires occurred during the spring of 2005. Large amount of O_3 precursors and aerosol were transported from the Korean peninsula to large part of northeastern China, under favorable synoptic weather conditions. The emissions from Korean forest fires were analyzed using satellite and ground-based measurement data to investigate their impact on the regional air quality. Higher concentrations of surface O_3 and CO as well as the ozone precursors (VOCs) were observed within the period of the Korean forest fires. It was the first recording of adverse air pollution effect resulted from Korean forest fires over northeastern China. Additionally, observations from the TOMS AI suggested that the smoky plume from the forest fire emissions could disperse and obscure a vast land area of the northeastern part of China under normal meteorological conditions.

This study provided the information to fill the gap in these two vacuum areas of the Eurasian continent. In addition, the impacts of open burning activities and forest fires from neighboring countries to China had been assessed and analyzed. It is of critical importance to monitor, on a long-term basis, chemically and radioactively important trace gases and aerosols, especially in undeveloped regions of China, so that their environmental implications can be reliably assessed. In this regard, the measurements from this study may serve as a baseline against which further changes can be compared and evaluated.

Appendix I) Typical backward air trajectory at Tengchong under the influences of eastern air mass

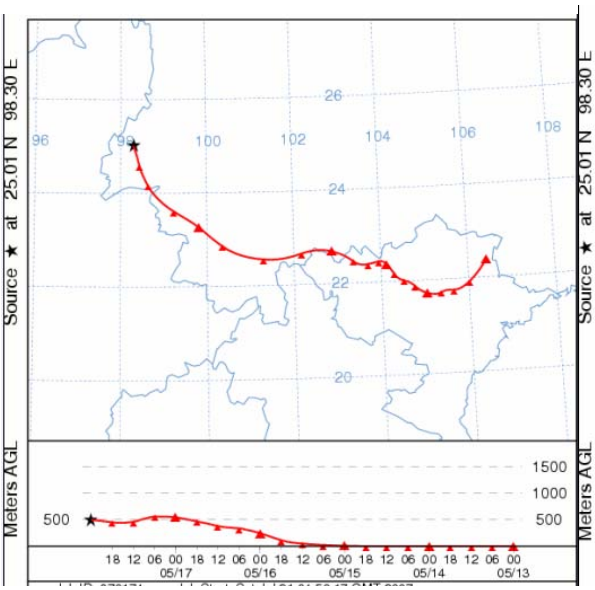

18 May 2004

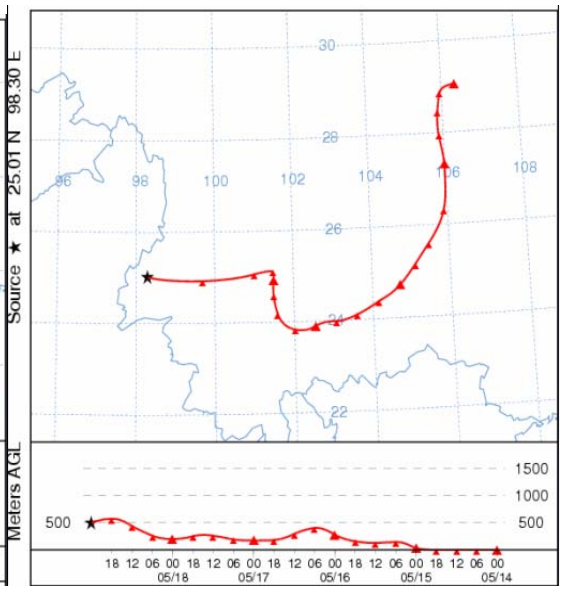

19 May 2004

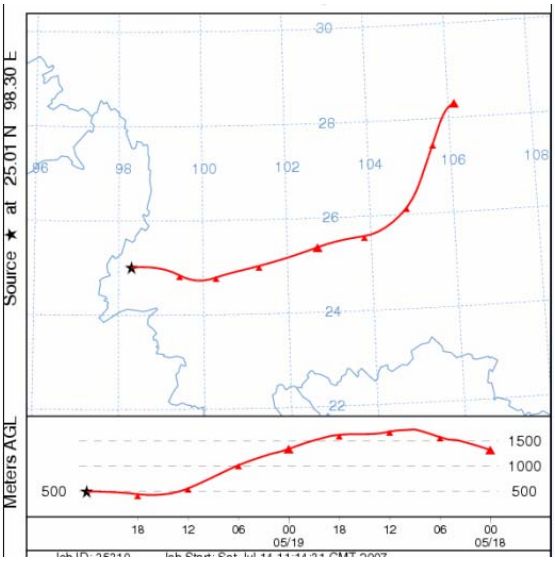

20 May 2004

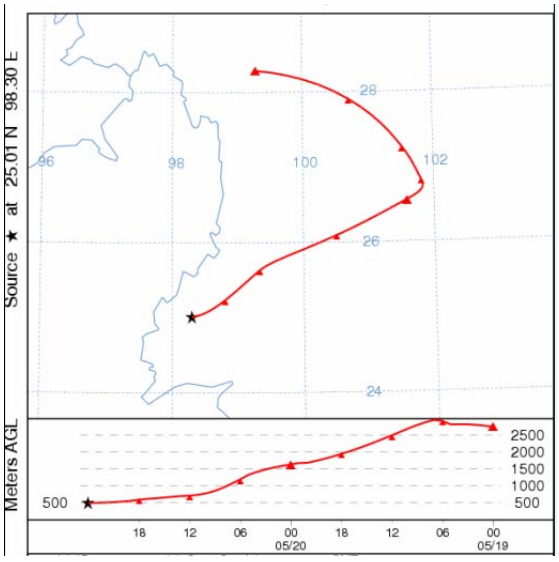

21 May 2004

Appendix II) Fire activities in Southeast Asia under the influence of eastern air mass

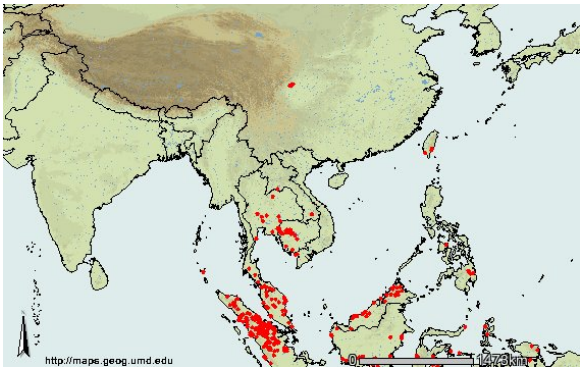

18 May 2004

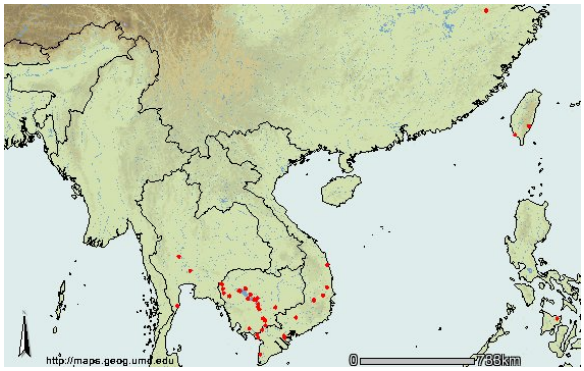

19 May 2004

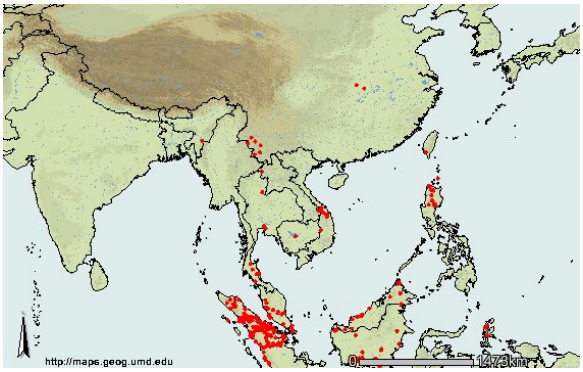

20 May 2004

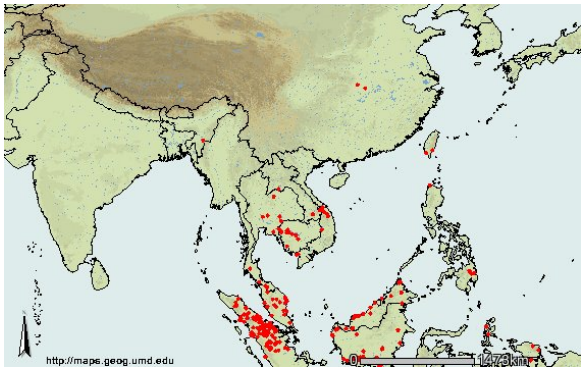

21 May 2004

References:

1. Allen, A.G. and A.H. Miguel, 1995. Biomass burning in the amazon: characterization of the ionic component aerosols generated from flaming and smouldering rain forest and ssavannah, *Environ. Sci. Technol.*, 29, 486-493.

2. Andreae, M.O., 1991. Biomass burning: Its history, use and distribution and its impact on environmental quality and global climate, in Global Biomass Burning: Atmospheric, Climatic, and Biospheric Implications, edited by J.S. Levine. *MIT Press, Cambridge, Mass., pp.3-21.*

3. Andreae, M.O. and P. Merlet, 2001. Emission of trace gases and aerosols from biomass burning, *Global biogeochemical Cycles*, 15(4), 955-966.

4. Austin, J. F. and R.P. Midgley, 1994. The climatology of the jet stream and stratospheric intrusions of ozone over Japan, *Atmos. Environ.*, 28, 39-52.

5. Cachier, H., J. Ducret, M.P. Bremond, A. Gaudichet, J.P. Lacaux, V. Yoboue, J. Baudet and J. Levine, 1991. Characterization of biomass burning aerosols in a savannah region of the Ivory Coast. Global Biomass Burning, *MIT press, Cambridge*, 174-180.

6. Cachier, H., C. Liousse, P. Buat-Menard and A. Gaudichet, 1995. Particulate content of savanna fire emission. *J. Atmos. Chem.*, 22, 123-148.

7. Cahoon, D.R., B.J. Stocks, J.S. Levine, W.R. Cofer III, and J.M. Pierson, 1994. Satellite analysis of the severe 1987 forest fire in northern China and southeastern Siberia, *J. Geophys. Res.*, 99, 18627-18638.

8. Carmichael, G. R., Y. Tang, G. Kurata, I. Uno, D.G. Streets, N. Thongboonchoo, J.H. Woo, S. Guttikunda, A. White, T. Wang, D.R. Blake, E. Altlas, A. Fried, B. Potter, M.A. Avery, G.W. Sachse, S.T. Sandholm, Y. Kondo, R.W. Talbot, A. Bandy, D. Thorton, and A.D. Clarke, 2003. Evaluating regional emission estimates using the TRACE-P observations, *J. Geophys. Res.*, 108(D21), 8810, doi:10.1029/2002JD003116.

9. Carter, W.P.L., 1994. Development of ozone reactivity scales for volatile organic compounds, *J. Air Waste Manage.*, 44, 881-899.

10. Chan, C.Y., L.Y. Chan, Y.G. Zheng, J.M. Harris, S.J. Oltmans and S. Christopher, 2001. Effects of 1997 Indonesian forest fires on tropospheric ozone enhancement, radiative forcing, and temperature change over the Hong Kong region, *J. Geophys. Res.*, 106, 14,875-14,885.

11. Chan, C. Y., L.Y. Chan, K.S. Lam, and Y.S. Li, 2002. Effects of Asian air pollution transport and photochemistry on carbon monoxide variability and ozone production in subtropical coastal south China. *J. Geophys. Res.*, 107, D24, 4746, doi: 10.1029/2002JD002131.

12. Chan, C.Y., L.Y. Chan, W.L. Chang, Y.G. Zheng, H. Cui, X.D. Zheng, Y. Qin, and Y.S. Li, 2003a. Characteristics of a tropospheric ozone profile and implications for the origin of ozone over subtropical China in the spring of 2001, *J. Geophys. Res.*, 108, D20, 8800, doi:10.1029/2003JD003427.

13. Chan, C.Y., L.Y. Chan, H. Cui, X.D. Zheng, Y.G. Zheng, Y. Qin, and Y.S. Li, 2003b. Origin of the springtime tropospheric ozone maximum over east China at LinAn in 2001, *Tellus B*, 982-992.

14. Chan, C.Y., L.Y. Chan, J.M. Harris, S.J. Oltmans, and D.R. Blake, 2003c. Characteristics of Biomass Burning Emission Sources, Transport and Chemical Speciation of Enhanced Springtime Ozone Profile over the Troposphere of Hong Kong Area. *J. Geophys. Res., 108(0)*, doi: 10.1029/2001JD001555.

15. Chan, C.Y., K.H. Wong, Y.S., Li, L.Y. Chan and X.D. Zheng, 2006. The effect of Southeast Asia fir activities on tropospheric ozone, trace gases and aerosols at a remote site over the Tibetan Plateau of Southwest China. *Tellus, 58B, 310-318.*

16. Chan, L.Y., C.Y. Chan, and Y. Qin, 1998. Surface ozone pattern in Hong Kong, *J. Appl. Meteorol.*, 37, 1153-1165.

17. Chan L.Y., C.Y. Chan, H.Y. Liu, S. Christopher, S.J. Oltmans and J.M. Harris, 2000. A case study on the biomass burning in Southeast Asia and enhancement of tropospheric ozone over Hong Kong, *Geophys. Res. Lett.*, 27, 1479-1482.

18. Choi, Y., S. Elliott, I.J. Simpson, D.R. Blake, J.J. Colman, M.K. Bubey, S. Meinardi, F.S. Rowland, T. Shirai and F.A. Smith, 2003. Survey of whole air data from the second airborne biomass burning and lightning experiment using principal component analysis, *J. Geophys. Res.*, 108, 4163, dio:10.1029/2002JD002841.

19. Chow, J.C., 1995. Measurement methods to determine compliance with ambient air quality standards for suspended particles. Journal of the Air and Waste Mangement Association, 45, 320-382.

20. Christopher, D.E. and E.D. Kimberly, 1996. Survey of fires in Southeast Asia and India during 1987. Global Biomass Burning Vol. 2, edited by J. Levin, *MIT Press, Cambridge, Mass*, pp.663-670.

21. Christopher, S.A., J. Chou, R.M. Welch, D.V. Kliche and V.S. Connors, 1998. Satellite investigations of fire, smoke, and carbon monoxide during April 1994 MAPS mission: Case studies over tropical Asia. *J. Geophys. Res.*, 103, 19,327-19,336.

22. Chung, Y.S., 1986. Air pollution detection by satellites: The transport and deposition of air pollutants over oceans. *Atmos. Environ., 25a, 2457-2471*.

23. Cofer, W.R., E.L. Winstead, B.J., Stocks, L.W. Overbay, J.G. Goldammer, D.R. Cahoon, and J.S. Levine, 1996. Emissions from boreal forest fires: Are the atmospheric impacts underestimated?, in Biomass Burning and Global Change, edited by J.S. Levine. *MIT Press, Cambridge, Mass.* pp. 834-839.

24. Crawford, J., D. Davis, G. Chen, J. Bradshaw, S. Sandholm, Y. Kondo, S. Liu, E. Browell, G. Gregory,. B. Anderson, G. Sachse, J. Collins, M. Barrick, D. Blake, R. Talbot and H. Singh, 1997. An assessment of ozone photochemistry in the extra tropical western North Pacific: Impact of continental outflow during the late winter/early spring. *J. Geophys. Res.*, 102, 28,469-28,488.

25. Crutzen, P.J. and M.O. Andreae, 1990. Biomass burning in the tropics. Impact on atmospheric chemistry and biogeochemical cycle, *Science*, 250, 1669-1678.

26. Danielsen, E.F., 1994. Stratosphere-troposphere exchange based on radioactivity, ozone and potential vorticity, *J. Atmos. Sci.*, 25, 502-518.

27. Debaje, S. B., S.J. Jeyakumar, K. Ganesan, D.B. Jadhav and P. Seetaramayya, 2003. Surface ozone measurements at tropical rural coastal station Tranquebar, India. *Atmos. Environ.* 37, 4911–4916.

28. Derwent, R. G., P.G. Simmonds, S. Seuring and C. Cimmer, 1998. Observation and interpretation of the seasonal cycles in the surface concentrations of ozone and carbon monoxide at Mace Head, Ireland from 1990 to 1994. *Atmos. Environ*, 32, 144–157.

29. Ding, Y., 1994. *Monsoons over China*. Kluwer Academic Publishers, The Netherlands.

30. Draxler, R.R. and G.D., Hess, 1997. Description of the HYSPLIT_4 modeling system. *NOAA Technical Memo ERL ARL-224*, Decemeber.

31. Duan, F. K., X.D. Liu, T. Yu and H. Cachier, 2004. Identification and estimate of biomass burning contribution to the urban aerosol organic carbon concentrations in Beijing. *Atmos. Environ*., 38, 1275-1282.

32. Duncan, B.N., R.V. Martin, A.C. Staudt, R. Yevich and J.A. Logan, 2003. Interannual and seasonal variability of biomass burning emissions constrained by satellite observations, *J. Geophys. Res.*, 108 (D2), 4040.

33. Dwyer, E., J.M. Gregoire and J.P. Malingreau, 1988. A global analysis of vegetation fires using satellite images: spatial and temporal dynamics, *AMBIO*, 27, 175-181.

34. Echalar, F., A. Gaudichet, H. Cachier and P. Artaxo, 1995. Aerosol emissions by tropical forest and Savannah biomass burning: characteristic trace elements and fluxes. *Geophys. Res. Lett.*, 22, 3039-3042.

35. Elliott, S., D.R. Black, R.A. Ruce, C.A. Lai, I. McCreary, L.A. McNair, F.S. Rowland and A.G. Russell, 1997. Motoization of China implies changes in Pacific air chemistry and primary production, *Geophys. Res. Lett.*, 24, 2671-2674.

36. Fromm, M., J. Alfred, K. Hoppel, J. Hornstein, R., Bevilacqua, E. Shettle, R. Servranckx, Z. Li and B. Stocks, 2000. Obervations of boreal fires smoke in the stratosphere by POAM III, SAGE II, and lidar in 1998. *Geophys. Res. Lett.*, 1407-1410.

37. Granier, C., D. Brasseur, D. Erickson and S.H. Schneider, 1999. Atmospheric chemistry and climate, in *Atmospheric Chemistry and Global Change*, edited by Goy P. brasseur, J.J. Orlando, and G.S. Tyndall, Oxford Inv. Press, New York.

38. Herman, J.R., P.K. Bhartia, O. Torres, C. Hsu, C. Seftor, and E. Celarier, 1997. Global distribution of UV-absorbing aerosols from NIMBUS-7/TOMS data. *J. Geophys. Res.*, 102, 16,911-16,922.

39. Higgins K.F., A.D. Kruse and J.L. Piehl, 1989. Prescribed burning guidelines in the Northern Great Plains, version 16JUL97. US Fish and Wildlife Service, Cooperative Extension Service, South Dakota State University, US Department of Agriculture EC 760. Jamestown, ND: Northern Prairie Wildlife Research Center; 1989, home page: http://www.npwrc.usgs.gov/resource/tools/burning/burning.htm

40. Ho, K.F., S.C. Lee, C.K. Chan, J.C. Yu, J.C. Chow and X.H. Yao, 2003. Characterization of chemical species in $PM_{2.5}$ and PM_{10} aerosols in Hong Kong, *Atmos. Environ.*, 37, 31-39.

41. Ito, A., and L.E. Penner, 2004. Global estimates of biomass burning emissions based on satellite imagery for the year 2000, *J. Geophys. Res.*, 109, D14S05, doi:10.1029/2003JD004423

42. Jacob, D. J., J. Crawford, M. M. Kleb, V. S. Connors, R. J. Bendura, J. L. Raper, G. W. Sachse, J. Gille, L. Emmons, and J. C. Heald, 2003. Transport and chemical evolution over the Pacific (TRACE-P) mission: Design, execution, and first results, *J. Geophys. Res.*, 108(D20), 8781, doi:10.1029/2002JD003276.

43. Kajii, Y., H. Akimoto, Y. Komazaki, S. Tanaka, H. Mukai, K. Murano, and J.T. Merrill, 1997. Long-range transport of ozone, carbon monoxide, and acidic trace gases at Oki Island, Japan, during PEM-WEST B/PEACAMPORT B campaign, *J. Geophys. Res., 102, 28637-28649.*

44. Kajii, Y., S. Kato, D.G. Streets, N.Y. Tsai, A. Shvidenko, S. Nilsson, I. McCallum, N.P. Minko, N. Abushenko, D. Altyntsev, and T. Khodzer, 2002. Boreal forest fires in Siberia in 1998: Estimate of area burned and emissions of pollutants by advanced very high resolution radiometer satellite data, *J. Geophys. Res.*, 107, D24, doi:10.1029/2001JD001078.

45. Kasischke, E.S. and B.J. Stocks, 2000. Fire, Climate change, and carbon cycling in the boreal forests, *Ecol. Stud*., 138, 461 pp.

46. Kato, S., P. Pochanart, J. Hirokawa, Y. Kajii, H. Akimoto, Y. Ozaki, K. Obi, T. Katsuno, D.G. Streets, and N.P. Minko, 2002. The influence of Siberian forest fires on carbon monoxide concentrations at Happo, Japan. *Atmos. Environ., 36, 385-390.*

47. KBS world Radio: http://rki.kbs.co.kr/english/news

48. Kennish, M.J. (Ed.), 1994. *Practical Handbook of Marine Science*. CRC Press, Boca Raton.

49. Kirchhoff, V.W.J.H., 1998. Surface ozone measurements in Amazonia, *J. Geophys. Res.*, 93, 1469-1476.

50. Lacaux, J.P., H. Cachier and R. Delmas, 1993. Biomass burning in Africa: In: Crutzen P.J., Goldammer J.G. (Eds.), Fire in the Environment, Wiley, *Chichester. Dahlem Workshop Report on Environmental Sciences Research,* ES 13 pp159-191.

51. Lee, K.H., J.E. Kim and Y.J. Kim 2005. Impact of the smoke aerosol from Russian forest fires on the atmospheric environment over Korea during May 2003, *Atmos. Environ.,* 39, 85-99.

52. Lewis, C.W., R.E. Baumgardner, R.K. Stevens, L.D. Claxt and J. Lewtas, 1988. Contribution of woodsmoke and motor vehicle emissions to ambient aerosol mutagenicity. *Environ. Sci. Technol.*, 22, 968-971.

53. Lemieus, P.M., C.L. Christopher and D.A. Santoianni, 2004. Emissions of organic air toxics from open burning: a comprehensive review, *Prog. Energ. Combust.*, 30, 1-32.

54. Liu, H., W.L. Chang, S.J. Oltmans, L.Y. Chan and J.M. Harris, 1999. On springtime high ozone events in the lower troposphere from Southeast Asian biomass burning, *Atmos. Environ.*, 33, 2403-2410.

55. Liu, S.C., M., Trainer, F.C. Fehsenfeld, D.D. Parrish, E.J. Williams, D.W. Fahey, G. Hubler and P.C. Murphy, 1987. Ozone production in the rural troposphere and the implications for regional and global ozone distributions, *J. Geophys. Res.*, 92, 4191-4207.

56. Maenhaut, W., I. Salma, J. Cafmeyer, H.J. Annegarn and M.O. Andreae, 1996. Regional atmospheric aerosol composition and sources in the eastern Transvaal, South Africa and impact of biomass burning, *J. Geophys. Res.,* 101 (D19), 23631-23650.

57. Mann, S. and M.O. Andreae, 1994. Emission of Methyl Bromide from biomass burning. Science, 263, 1255-57.

58. Masters, G.M., *Introduction to Environmental Engineering and Science*, Prentice-Hall, Old Tappan, N.J., 1998.

59. Murao, N., S. Ohta, F. Naritaka, and M. Mizoguchi, 1990. The cause of elevated ozone concentrations in Sapporo, *Atmos. Environ.*, 24, 1501-1507.

60. Oltmans, S. J. and H. II. Levy, 1994. Surface ozone measurements from a global network. *Atmos. Environ.* 28, 9–24.

61. Oltmans S.J., B.J. Johnson, J.M. Harris and A.M. Thmopson, 2004. Tropospheric ozone over the North Pacific ozonesonde observations, *J. Geophys. Res.*, 109, doi: 10.1029/2003JD003466.

62. Pochanart, P., J. Hirokawa, Y. Kajii, and H. Akimoto, 1999. Influence of regional-scale anthropogenic activity in northeast Asia on seasonal variations of surface ozone and carbon monoxide observed at Oki, Japan. *J. Geophys. Res.*, 104, 3621-3631.

63. Pochanart, P., J. Kreasuwun, P. Sukasem, W. Geeratithadaniyom and M.S. Tabucanon, 2001. Tropical tropospheric ozone observed in Thailand. *Atmos. Environ.* 35, 2657–2668.

64. Russo, R.S., R.W. Talbot, J.E. Dibb, E. Scheuer, G. Seid, C.E. Jordan, H.E. Fuelberg, G.W. Sachse, M.A. Avery, S.A. Vay, D.R. Blake, N.J. Blake, E. Atlas, A. Fried, S.T. Sandholm, D. Tan, H.B Singh, J. Snow, J. Snow and B.G. Heikes, 2003, Chemical composition of Asian continental outflow over the western Pacific: Results from Transport and Chemical Evolution over the Pacific(TRACE-P), *J. Geophys. Res.*, 108(D20), 8804, doi:10.1029/2002JD003184.

65. Shvidenko, A.Z. and S. Nilsson, 2000. Extent, distribution, and ecological role of fire in Russian forests, in Fire, Climate Change, and Carbon Cycling in the Boreal Forests, edited by E.S. Kasischke, *Ecol. Stud.*, 138, 132-150.

66. Sunwoo, Y., G.R. Carmichael and H. Ueda, 1994. Characteristics of background surface ozone in Japan, *Atmos. Environ.*, 28, 25-37.

67. Sze, N.D., 1977. Anthropogenic CO emissions: Implications for the CO-OH-CH_4 cycle, *Science*, 195, 673-675.

68. Talbot, R.W., 1997, Chemical characteristics of continental outflow from Asia to the Troposphere over the Western Pacific Ocean during February – March 1994: Results from PEM-West B, *J. Geophys. Res.*, 102(D23), 28255-28274.

69. Tang, J., X.S. Li and Y.C. Zhao, 1996. Preliminary analysis on the surface ozone observed at Mt.Waliguan. In: *Variations of Ozone over China and Its Impacts on Climate and Environment (I)* (ed Xiuji Zhou). Meteorological Press, Beijing, China.

70. Tanimoto, H., U. Kajii, J. Hirokawa, H, Akimoto and N.P. Minko, 2000. The atmospheric impact on boreal forest fires in far eastern Siberia on the seasonal variation of carbon monoxide: Obervations at Rishiri, a northern remote island in Japan. *Geophys. Res. Lett.*, 27, 4073-4076.

71. Tazaki, K., Wakimoto, R., Minami, Y., and Yamamoto, M., 2004. Transport of carbon-bearing dusts from Iraq to Japan during Iraq's War, *Atmos. Environ.*, 38, 2091-2109.

72. The Korea Times: http://times.hankooki.com

73. Tsutsumi, Y. and Y. Makino, 1994. Vertical distribution of the tropospheric ozone over Japan: the origin of the ozone peaks, *J. of Meteorol. Soc. Jpn*, 73, 1041-1058.

74. UNEP and C4 (United Nations Environment Programme and Centre for Clouds, Chemistry and Climate). 2002. *The Asian Brown Cloud: Climate and Other Environmental Impacts.* UNEP, Nairobi.

75. Wang, X.M., G.Y. Sheng, J.M. Fu, C.Y. Chan, S.C. Lee, L.Y. Chan and Z.S. Wang, 2002. Urban roadside aromatic hydrocarbons in three cities of the Pearl River Delta, People's Republic of China, *Atmos. Environ.*, 36, 5141-5148.

76. Wang, T., V. T. F. Cheung, M. Anson, and Y.S. Li, 2001. Ozone and related gaseous pollutants in the boundary layer of eastern China: Overview of the recent measurements at a rural site. *Geophys. Res.Lett.* 28 (12), 2373–2376.

77. Wang, T., A. J. Ding, D.R. Blake, W. Zahorowski, C.N. Poon and Y.S. Li, 2003, Chemical characterization of the boundary layer outflow of air pollution to Hong Kong during February–April 2001, *J. Geophys. Res.*, 108(D20), 8787, doi:10.1029/2002JD003272.

78. Wang ,T. and J.Y.H., Kwok, 2003. Measurement and analysis of a mutiday photochemical smog episode in the Pearl River Delta of China, *J. Appl. Meteorol.*, 45, 404-416.

79. Wang, T., H. Guo and D.R. Blake, 2005. Measurements of trace gases in the inflow of South China Sea background air and outflow of regional pollution at Tai O, Southern China, *J. Atmos. Chem.*, 52, 295-317.

80. Westphal, D.L. and O.B. Toon, 1991. Simulations of microphysical, radioactive, and dynamical processes in a continental-scale forest fire smoke plume. *J. Geophys. Res.*, 96, 22,379-22,400.

81. Wong, K.H., L.Y. Chan and Y.S. Li, 2006. Effects of abnormal crude oil open burnings in Middle East and tropospheric ozone enhancement over China during TAPTO-China period, *Geophys. Res.Lett.* (submitted).